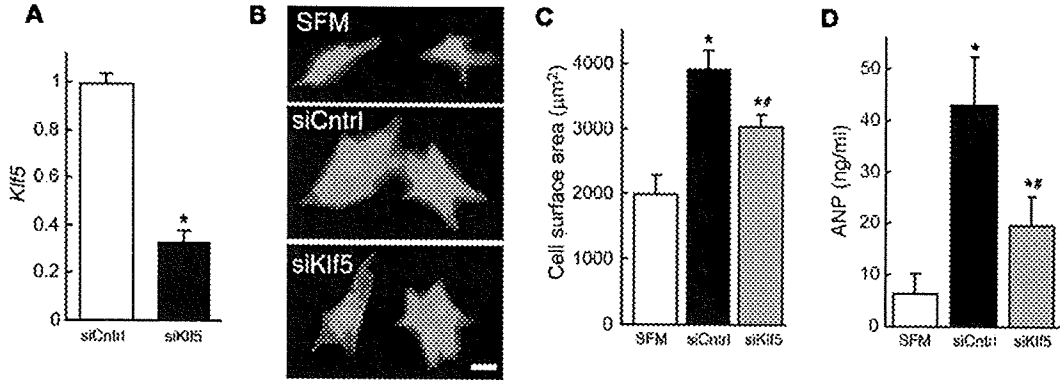

Figure 5

KLF5 controls expression of paracrine factors in cardiac fibroblasts that mediate cardiomyocyte hypertrophy. (**A**) siRNA-mediated knockdown of *Klf5* in cardiac fibroblasts. *Klf5* levels were normalized to those in cells transfected with the control siRNA (siCntrl). **P* < 0.01 versus siCntrl. (**B–D**) Cultured cardiomyocytes were incubated with serum-free medium (SFM) or conditioned medium prepared from cardiac fibroblasts transfected with control or *Klf5* siRNA for 48 hours. (**B**) Representative cardiomyocytes are shown stained for sarcomeric α-actinin (green) and nuclei (Hoechst 33258, blue). Scale bar: 10 μm. (**C**) Cell surface areas of 100 cells from each group. **P* < 0.01 versus cells treated with SFM; #*P* < 0.05 versus cells treated with medium conditioned by siCntrl transfectants. (**D**) ANP concentrations in culture medium conditioned by cardiomyocytes. **P* < 0.05 versus SFM; #*P* < 0.05 versus siCntrl.

Cardiac fibroblasts are essential for adaptive responses to severe pressure overload. Next we assessed the importance of cardiac fibroblasts in the adaptive responses of the myocardium for maintenance of cardiac function. *Klf5*$^{fl/fl}$ and *Klf5*$^{fl/fl}$;*Postn-Cre* mice were subjected to HI-TAC, which we previously found to induce cardiac dysfunction within 2 weeks (Supplemental Figures 1 and 2). After 10 days of HI-TAC, *Klf5*$^{fl/fl}$;*Postn-Cre* mice were visibly emaciated, and their body weights were correspondingly diminished (data not shown). In addition, mortality among *Klf5*$^{fl/fl}$;*Postn-Cre* mice was significantly higher than among *Klf5*$^{fl/fl}$ mice after 14 days of HI-TAC (Figure 7A). Pulmonary edema and/or hemorrhage were noted in most of the dead *Klf5*$^{fl/fl}$;*Postn-Cre* mice, and even in those that survived, lung weights were significantly increased due to pulmonary congestion and alveolar edema (Figure 7, B and C). Many *Klf5*$^{fl/fl}$;*Postn-Cre* mice also exhibited shallow, rapid breathing characteristic of heart failure. Nonetheless, cardiac hypertrophy and fibrosis were markedly attenuated in *Klf5*$^{fl/fl}$;*Postn-Cre* mice, though LV luminal diameters were markedly increased (Figure 7, D–G). Because of the fragility of *Klf5*$^{fl/fl}$;*Postn-Cre* mice, systematic echocardiographic analysis could not be performed, as even a minimum dose of anesthetic was lethal. However, the 1 *Klf5*$^{fl/fl}$;*Postn-Cre* mouse that survived the anesthesia showed marked LV dilation and diminished systolic function (Figure 7H). Apparently, expression of KLF5 by cardiac fibroblasts is necessary for the adaptive and protective activities that take place within the myocardium in response to severe pressure overload.

Finally, we tested whether IGF-1 is required for the cardioprotective responses to pressure overload by using JB1, a peptide IGF-1 receptor antagonist, to inhibit IGF-1 signaling in vivo (40). JB1 did not affect survival, cardiac function, heart weights, or cardiac histology in sham-operated control mice (data not shown). In mice subjected to HI-TAC, by contrast, JB1 administration led to the emaciation and shallow, rapid breathing characteristic of heart failure as well as early death (Figure 8A). In JB1-treated mice subjected to HI-TAC, the lung weights were significantly increased (Figure 8, B and C), cardiac hypertrophy was attenuated (Figure 8, D–F), and the left ventricle was significantly enlarged (Figure 8, D and F). Moreover, systolic function was impaired more than in vehicle-treated mice (Figure 8F), indicating that JB1 exacerbated the heart failure. IGF-1 secreted from cardiac fibroblasts thus appears to be a crucial mediator of the cardioprotective response to severe pressure overload.

Discussion

The results of the present study clearly demonstrate that cardiac fibroblasts play essential roles in cardioprotection and cardiomyocyte hypertrophy, at least in part by producing paracrine factors, including IGF-1. Based on the observation that in addition to extracellular matrix proteins, cardiac fibroblasts produce a variety of paracrine factors — some of which can induce hypertrophic responses in vitro — it has been postulated that an interplay between cardiomyocytes and fibroblasts is involved in cardiac hypertrophy and pathology (2, 3). However, the potential requirement for fibroblasts in the cardiac response to pathological stress in vivo has not been fully appreciated. Our study provides clear evidence that cardiac fibroblasts functionally contribute to the adaptive response to pressure overload in vivo. Particularly noteworthy is our finding that cardiac fibroblasts are absolutely required for protection of cardiac function in severe pressure overload. This means that cardiac fibroblasts are not mere bystanders acting only in fibrosis, but are crucial mediators of myocardial hypertrophy and adaptive responses in the heart. It was recently suggested that inappropriate angiogenesis plays an important role in heart failure (41). That finding, together with those summarized here, highlights the importance of the activities of the non-muscle cells residing in the myocardial interstitium. In addition to contributing to pathological remodeling, it is likely that these cells mediate homeostatic responses to physiological stress.

Our findings also indicate that KLF5 expressed in cardiac fibroblasts is a key regulator controlling the stress response in the myocardium. Moreover, the results obtained with cardiac fibroblast-specific *Klf5*-knockout mice suggest that IGF-1 produced by fibroblasts is also important for protective responses. These findings are consistent with the results of earlier studies of the effects

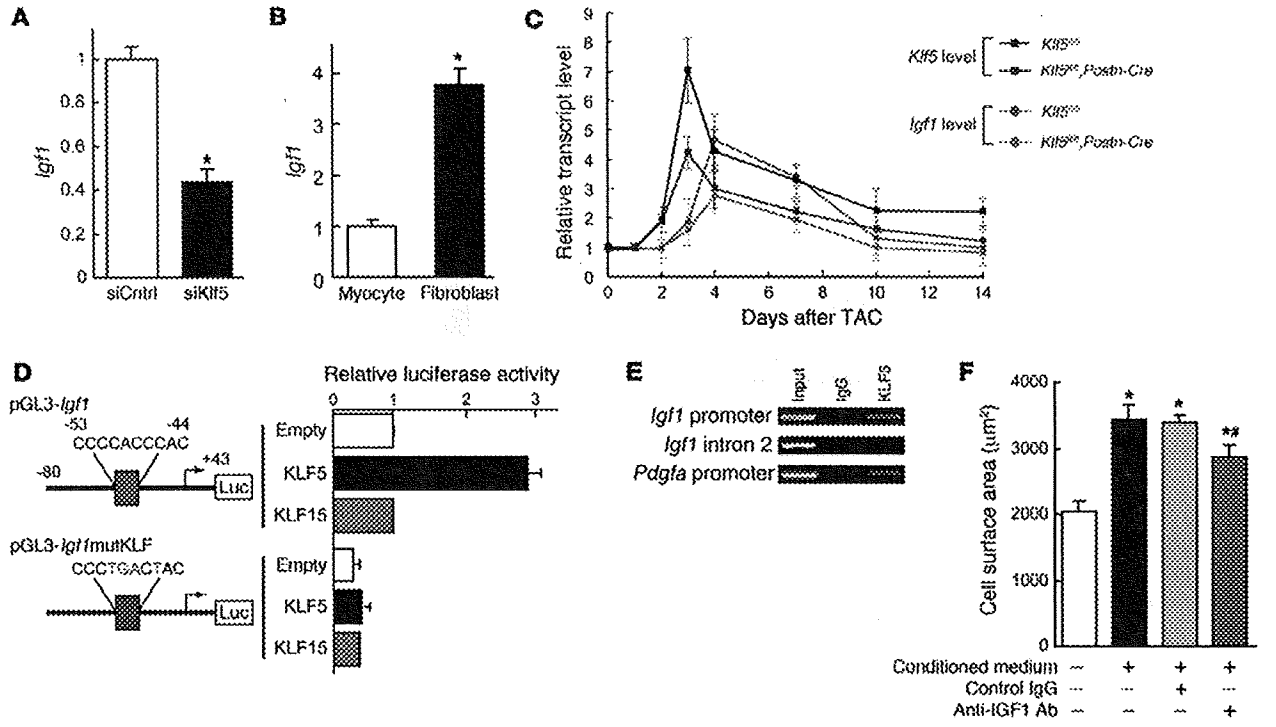

Figure 6

KLF5 transactivates the *Igf1* promoter. (**A**) KLF5 knockdown reduced *Igf1* expression in cardiac fibroblasts. KLF5 was knocked down as shown in Figure 5A. **P* < 0.01 versus siCntrl. (**B**) Fibroblast-selective expression of *Igf1*. *Igf1* mRNA levels in cultured cardiac fibroblasts were normalized to those of 18s rRNA and then further normalized with respect to those in cardiomyocytes. **P* < 0.01 versus cardiomyocytes. (**C**) Cardiac expression of *Klf5* and *Igf1* mRNA after LI-TAC in *Klf5*$^{fl/fl}$ and *Klf5*$^{fl/fl}$;*Postn-Cre* mice. Expression levels were normalized to those of 18s rRNA and then further normalized with respect to those in the hearts before TAC. (**D**) Reporter analysis of KLF5-depedent transactivation of the *Igf1* promoter. Luciferase reporter constructs driven by the wild-type *Igf1* promoter or a mutant promoter in which the potential KLF-binding site was mutated were cotransfected with either empty vector or a vector harboring *Klf5* or *Klf15*. Data are representative of 3 independent experiments. (**E**) ChIP assays of KLF5 binding to the *Igf1* and *Pdgfa* promoters. An intronic region of *Igf1* that does not contain a KLF-binding motif served as a negative control. (**F**) Effects of neutralizing IGF-1 on the cardiotrophic activity of fibroblast-conditioned medium. An antibody against IGF-1 (30 μg/ml) or normal IgG was added to the conditioned medium, after which the effect of the medium on cardiomyocyte surface area was analyzed. **P* < 0.01 versus cells treated with SFM; #*P* < 0.01 versus cells treated with fibroblast-conditioned medium.

of transgenic overexpression of IGF-1 and IGF-1 receptor in cardiomyocytes, which were also suggestive of IGF-1's role in physiological hypertrophy and cardiac protection (42–46). Thus IGF-1 produced locally by fibroblasts appears to be a key mediator of cardiac hypertrophy and myocardial protection against pressure overload.

The present study identified *Igf1* as the target of KLF5 in fibroblasts involved in the cardiac adaptive response. However, KLF5 also likely controls the expression of genes other than *Igf1* and *Pdgfa*, including those encoding paracrine factors involved in regulating fibroblast function (Supplemental Table 1). We would therefore expect future studies of the gene networks controlled by KLF5 in cardiac fibroblasts to shed additional light on their homeostatic and pathological functions. In that regard, it will also be important to analyze the possible interplay between KLF5 and other members of the KLF family. Previous studies have demonstrated the functional roles played by several KLFs in the heart (34, 35, 47, 48). For instance, KLF15 negatively regulates cardiac fibrosis (34). It is therefore conceivable that networks of KLFs contribute to the myocardial responses to stress. Finally, our results suggest that therapeutic modulation of cardiac fibroblast function may represent a novel approach to the prevention and/or treatment of heart failure.

Methods

For experimental procedures not described herein, see Supplemental Methods.

Animals. Mice were housed in temperature-controlled rooms with a 12-hour light/12-hour dark cycle. All experiments were approved by the University of Tokyo Ethics Committee for Animal Experiments and strictly adhered to the guidelines for animal experiments of the University of Tokyo.

Generation of Klf5-floxed mice. A 12-kb *Klf5* fragment containing exons 1–3 was used to construct the targeting vector. The scheme for construction of the targeting vectors is shown in Supplemental Figure 5. The targeting construct was introduced into ES cells by electroporation, and G418-resistant clones were then examined for homologous recombination using Southern blot analysis with appropriate 3′ probes. Six ES clones that contained the correctly targeted *Klf5* locus were obtained, and 2 were injected into 129/Sv blastocysts to obtain chimeric mice. Male chimeras were bred with female transgenic mice expressing the enhanced site-specific recombinase FLP to remove the FRT-flanked neomycin cassette to generate heterozygous floxed *Klf5* (*Klf5*$^{fl/+}$) mice. *Klf5*$^{fl/+}$ mice were then backcrossed with C57BL/6 mice using the marker-assisted speed congenic method (49). The mice were genotyped by Southern blot analysis or PCR. Southern blot analysis was performed after *Hind*III digestion using a 396-bp PCR-amplified

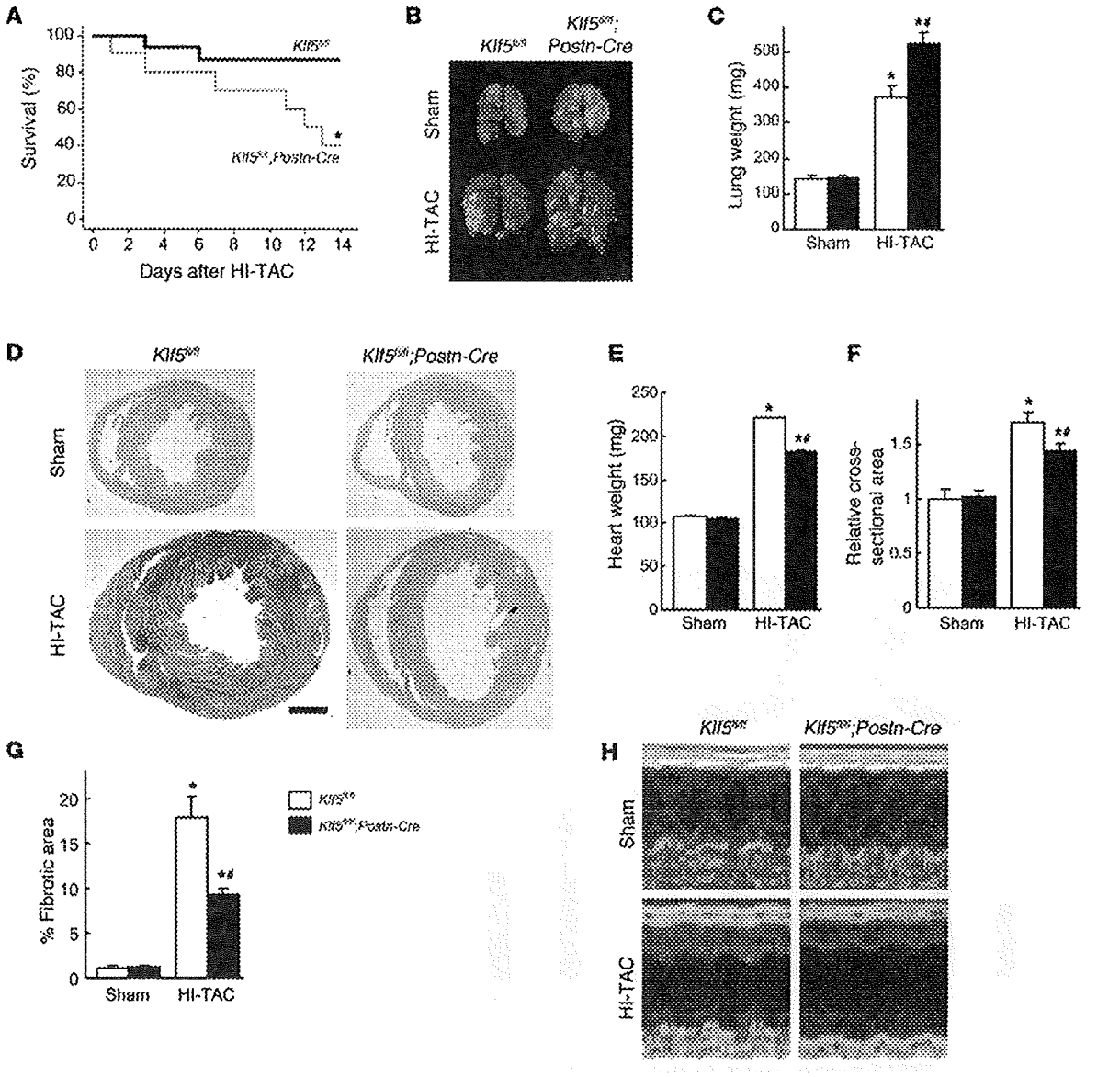

Figure 7

Cardiac fibroblasts are essential for the protective response elicited by severe pressure overload. (**A**–**H**) *Klf5*$^{fl/fl}$ and *Klf5*$^{fl/fl}$;*Postn-Cre* mice were subjected to HI-TAC or sham operation. (**A**) Kaplan-Meier survival analysis of *Klf5*$^{fl/fl}$ (n = 16) and *Klf5*$^{fl/fl}$;*Postn-Cre* (n = 10) mice after HI-TAC. *P < 0.05 versus *Klf5*$^{fl/fl}$. (**B**) Representative pictures of lungs 2 weeks after the operations. Note the severe lung edema in *Klf5*$^{fl/fl}$;*Postn-Cre* mice subjected to HI-TAC. (**C**) Lung weights in *Klf5*$^{fl/fl}$ (n = 5) and *Klf5*$^{fl/fl}$;*Postn-Cre* (n = 3) mice 2 weeks after the operations. (**D**) Representative low-magnification views of H&E-stained heart sections 2 weeks after the operations. Scale bar: 1 mm. (**E**–**G**) Heart weight/body weight ratios (**E**), relative cross-sectional areas of cardiomyocytes (**F**), and fibrotic areas (**G**) in *Klf5*$^{fl/fl}$ (n = 5) and *Klf5*$^{fl/fl}$;*Postn-Cre* (n = 3) mice 2 weeks after the HI-TAC operation. *P < 0.01 versus sham control of the same genotype; #P < 0.05 versus *Klf5*$^{fl/fl}$ mice subjected to HI-TAC. (**H**) M-mode echocardiographic tracings obtained 2 weeks after the operations.

probe for hybridization (Supplemental Figure 5). The probe for intron 1 was made by PCR using primers 5′-TGTCGTGGTGCTTTGAGAAG-3′ and 5′-TATCTTCCAGGCCCTGATTG-3′. PCR for genotyping was performed with primers A (5′-GCATCAGGAGGGTTTCATGT-3′) and B (5′-GTCTCGGCCTCATTGCTAAG-3′), which yielded 164-bp and 331-bp products for wild-type and floxed *Klf5* alleles, respectively.

Quantification of Cre-mediated recombination. Competitive PCR was performed to calculate the relative deletion frequency using primers A, B, and C (5′-TGACCCATTACCGAATCTACTG-3′), which produced 331-bp and 250-bp bands for the floxed and floxed-out *Klf5* alleles, respectively. The respective abundances of the floxed and floxed-out *Klf5* alleles were analyzed using real-time PCR with the same primer sets. To calculate absolute numbers of alleles in a given cell sample, we used external standards containing known numbers of DNA fragments derived from *Klf5*-floxed and floxed-out alleles.

TAC model. TAC was performed as described previously (50). Briefly, mice (8–10 weeks old, 21–24 g body weight) were anesthetized by intraperitoneal injection of a mixture of xylazine (5 mg/kg) and ketamine (100 mg/kg).

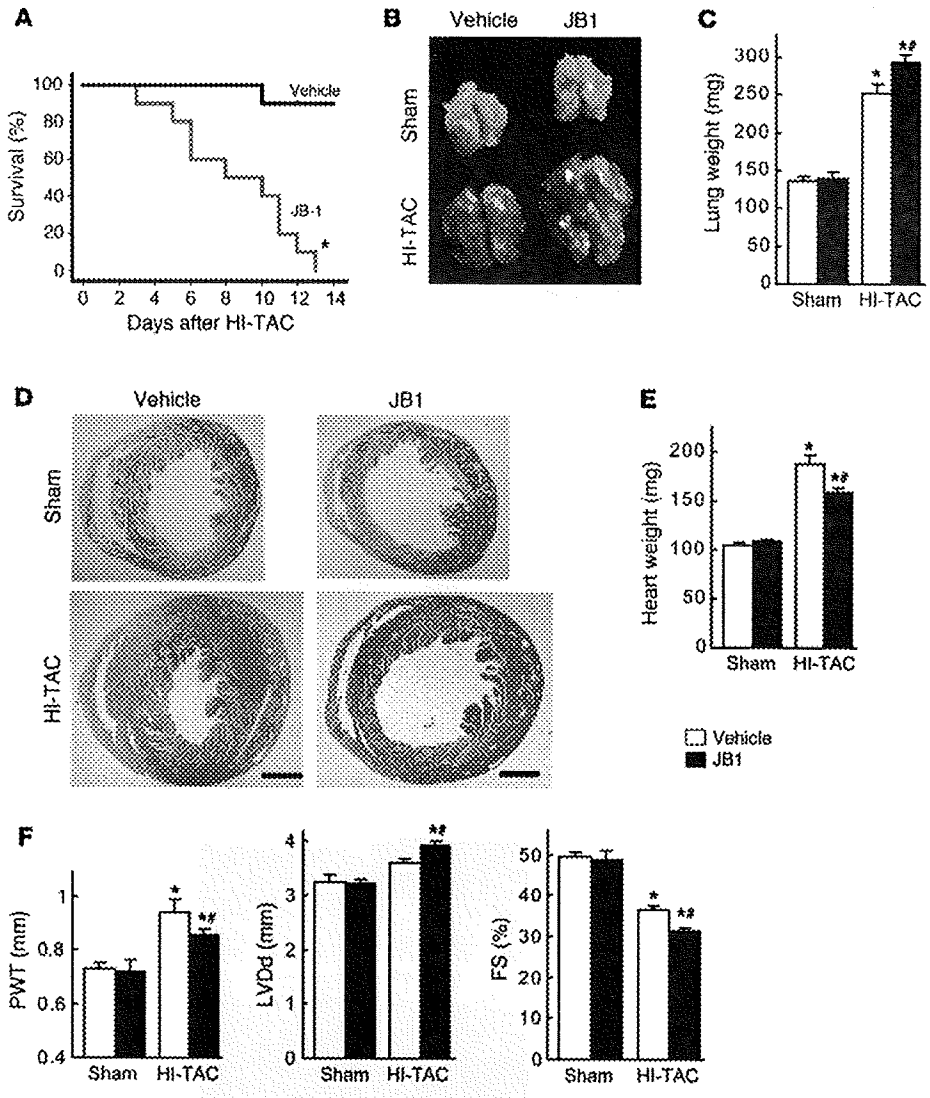

Figure 8
An IGF-1 receptor antagonist aggravates heart failure induced by severe pressure overload. (**A**) Kaplan-Meier survival analysis of wild-type mice treated with vehicle or JB1, a peptide IGF-1 receptor antagonist, after HI-TAC. $n = 10$ in each group. $^*P < 0.001$ versus vehicle. (**B**) Representative photographs of lungs taken 1 week after the operations. Note the severe lung edema in JB1-treated mice subjected to HI-TAC. (**C**) Lung weights in vehicle-treated and JB1-treated groups 1 week after the operations. $n = 5$ in each group. (**D**) Representative low-magnification views of H&E-stained heart sections 1 week after the operations. Scale bars: 1 mm. (**E**) Heart weights. (**F**) Echocardiographic analysis carried out 1 week after the operation. $^*P < 0.05$ versus sham controls in the same treatment group; $^\#P < 0.05$ versus vehicle controls subjected to HI-TAC.

The animals were then placed in a supine position, an endotracheal tube was inserted, and the animals were ventilated using a volume-cycled rodent ventilator with a tidal volume of 0.4 ml room air and a respiratory rate of 110 breaths/minute. The chest cavity was exposed by cutting open the proximal portion of the sternum. After the aortic arch between the innominate and left common carotid arteries was isolated, it was constricted with a 7-0 nylon suture tied firmly 3 times against a 25- or 27-gauge blunted needle for LI- and HI-TAC, respectively. Sham-operated mice underwent the identical surgical procedure, including isolation of the aorta, but without placement of the suture.

Administration of JB1, a peptide IGF-1 receptor antagonist. C57BL/6 mice (8–10 weeks old, 21–24 g body weight) were anesthetized by intraperitoneal injection of pentobarbital sodium (50 mg/kg). An incision was made in the midscapular region under sterile conditions, and an osmotic minipump (Alzet) containing either JB1 (BACHEM) dissolved in 0.15 mol/l NaCl and 1 mmol/l acetic acid or vehicle only was implanted. The delivery rate was 1 mg/kg/d for 14 days.

Echocardiography. Animals were lightly anesthetized with 2,2,2-tribromoethanol (200 mg/kg) and set in a supine position. Two dimensional (2D) guided M-mode echocardiography was performed using an echocardiogram (model 4500, Sonos) equipped with a 15 to 6 L MHz transducer (Philips). The heart at the level of the LV papillary muscle was imaged in the 2D mode in the parasternal short-axis view with a depth setting of 2 cm. LV diastolic posterior wall thickness (PWT), LV diastolic dimensions (LVDd), and LV end-systolic dimensions (LVDs) were measured. LV fractional shortening (%FS) was calculated as (LVDd – LVDs)/LVDd × 100.

Histological analysis. Heart sections were prepared as described previously (14) and stained with H&E for overall morphology. Immunohistochemical staining of KLF5 was performed using an anti-KLF5 monoclonal antibody (KM1784). A biotin-conjugated goat anti-rat antibody, streptavidin-conjugated horseradish peroxidase (Dako), and 3,3′-diaminobenzidine (DAB) were used to visualize labeling. For double staining of KLF5 and αMHC, we also used anti-αMHC monoclonal antibody CMA19 (51). Simple Stain AP(M) (Nichirei) and an Alkaline Phosphatase Substrate Kit I (Vector) were used to visualize labeling. To quantify cardiac interstitial fibrosis, we stained sections with elastic picrosirius red, after which images were captured with a digital camera and analyzed using Photoshop (Adobe) and Scion Image.

β-Galactosidase staining. Heart tissues were fixed for 12 hours at 4°C in PBS containing 0.4% glutaraldehyde, 0.01% Na deoxycholate, 0.1% NP40, 0.1 M $MgCl_2$, and 5 mM EGTA; rinsed 3 times for 30 minutes in PBS; and

then incubated for 24 hours at 37°C in a staining solution [1 mM $MgCl_2$, 20 mM $K_3Fe(CN)_6$, 20 mM $K_4Fe(CN)_6$, 1 mg/ml X-gal in PBS]. LacZ-stained sections were counterstained with nuclear fast red for nuclei, biotin-conjugated isolectin B4 (Vector) for ECs, and elastic picrosirius red for fibrosis.

Cardiomyocyte cross-sectional area. Heart sections were deparaffinized, rehydrated, and incubated for 1 hour at room temperature with FITC-labeled wheat germ agglutinin (Sigma-Aldrich) to visualize myocyte membranes. Regions that included the circular shapes of capillaries were selected from the epicardial side of the LV free walls. The mean cross-sectional area of cardiomyocytes was determined for each mouse from 60 to 80 cells.

RNA extraction and real-time PCR. Heart tissues were stored in RNAlater RNA stabilization reagent (QIAGEN) at 4°C. Total RNA was extracted using an RNeasy Fibrous Tissue Mini Kit (QIAGEN). First-strand cDNA synthesis was performed with 1 μg of total RNA, random hexamers, and SuperScript III Reverse Transcriptase (Invitrogen). Real-time PCR was performed using a QuantiTect SYBR Green PCR kit (QIAGEN) in a LightCycler (Roche). The expression level of each gene was normalized to that of 18s rRNA, which served as an endogenous internal control. The sequences of the PCR primers are shown in Supplemental Table 2.

Isolation of neonatal and adult cardiomyocytes and non-myocytes. Neonatal ventricles from 1-day-old ICR mice were separated and minced in ice-cold balanced salt solution, as described previously with minor modifications (52). To isolate cardiac cells, the tissues were incubated in a balanced salt solution containing 0.2% collagenase type 2 (Worthington Biochemical) for 6 minutes at 37°C with agitation. The digestion buffer was replaced 7 times, at which point the tissues were completely digested. The dispersed cells were incubated in 10-cm culture dishes for 80 minutes to remove non-myocytes. The unattached viable cells, which were rich in cardiomyocytes, were cultured on gelatin-coated dishes at 37°C in DMEM supplemented with 10% FBS and 10 μM cytosine 1-β-D-arabinofuranoside (Ara C) to inhibit fibroblast proliferation. Using this protocol, we consistently obtained cell populations containing at least 90%–95% cardiomyocytes. Non-myocyte cells that attached to the dishes were cultured in DMEM supplemented with 10% FBS and allowed to grow to confluence, then they were trypsinized and passaged at1:3. This procedure yielded cell cultures that were almost exclusively fibroblasts by the first passage. Experiments were carried out after 2 or 3 passages.

Adult cardiomyocytes were isolated using the Langendorff perfusion method as previously described (27). For isolation of non-myocyte-enriched cells, hearts were dissected free of vessels and atria, washed in ice-cold modified Krebs-Henseleit bicarbonate (KHB) buffer (pH 7.2) (Sigma-Aldrich), and quickly cut into pieces. The heart pieces were incubated in 5 ml of digesting solution (0.25 mg/ml Liberase TH [Roche] and 10 mM HEPES in balanced salt solution containing calcium and magnesium) for 8 minutes at 37°C with vigorous stirring. The supernatant was then added to 10 ml of ice-cold KHB. Five milliliters of fresh digesting solution was added to the remaining tissue fragments, and the digestion and sampling steps were repeated until all the tissue was dissolved. The collected cells were filtered through 35-μm nylon mesh (BD Falcon) and then used for flow cytometry. Levels of *Myh6* mRNA expression were much lower in the isolated cell populations than in normal whole hearts, indicating that the cell populations obtained using the method described here were enriched in non-myocytes (Supplemental Figure 15). Flow cytometric analysis (Figure 3) showed that the cell populations contained large fractions of fibroblasts and ECs.

Flow cytometric analysis and sorting. Single cells were isolated from adult hearts and incubated with PE-conjugated anti-Thy1 antibody (eBioscience), FITC-conjugated anti-CD31 antibody (BD Biosciences), and allophycocyanin-conjugated CD3e antibody (eBioscience), after which they were analyzed and sorted using a FACSAria II (BD Biosciences) and FlowJo software.

For analysis of β-galactosidase expression and the sorting of LacZ$^+$ cells, a FluoReporter LacZ Flow Cytometry Kit (Molecular Probes, Invitrogen) was used according to the manufacturer's recommendations. Cells were stained with the fluorogenic β-galactosidase substrate fluorescein di-β-D-galactopyranoside (FDG).

Production of medium conditioned by cardiac fibroblasts. Cardiac fibroblasts were grown to subconfluency in 10-cm dishes. The medium was then replaced with fresh serum-free DMEM, and the cells were incubated for additional 48 hours. The medium was then collected as conditioned medium.

siRNA. siRNA for *Klf5* and control siRNA were purchased from Dharmacon. Using Lipofectamine RNAiMax (Invitrogen), the siRNA at a final concentration of 20 nM in 10 ml of culture medium was transfected into mouse cardiac fibroblasts plated in 10-cm culture dishes. siRNA-mediated knockdown of *Klf5* did not affect mRNA expression levels in KLF family members that reportedly function in the cardiovascular system (e.g., *Klf2*, *Klf4*, *Klf10*, *Klf13*, and *Klf15*) (Supplemental Figure 16).

Morphometric studies of cells. Neonatal cardiomyocytes cultured in 3.5-cm dishes were maintained in serum-free DMEM for 24 hours, after which the culture medium was replaced with either fresh serum-free DMEM or medium conditioned by cardiac fibroblasts. To analyze the effects of neutralizing IGF-1, either anti-IGF-1 neutralizing antibody (Millipore) or control IgG (Sigma-Aldrich) was then added, and the cells were cultured for an additional 24 hours. To analyze the effects of growth factors, cells were first cultured for 24 hours in serum-free DMEM. The medium was then replaced with serum-free DMEM containing vehicle, IGF-1 (Wako), or PDGF-A (R&D Systems), and the cells were cultured for an additional 24 hours. The cells were then fixed in 2% paraformaldehyde and permeabilized for 10 minutes with 0.5% Triton X-100 (Sigma-Aldrich) in PBS, after which they were incubated in PBS containing 1% bovine serum albumin for 10 minutes to block nonspecific staining. They were then incubated with anti–sarcomeric α-actinin antibody (Sigma-Aldrich), followed by treatment with an Alexa-conjugated secondary antibody. Cardiomyocyte size was determined by measuring the surface area of sarcomeric α-actinin–positive cells.

Enzyme-linked immunoassay. To analyze secretion of ANP, cardiomyocytes were cultured in the serum-free DMEM for 24 hours and then stimulated with fresh serum-DMEM or medium conditioned by cardiac fibroblasts for 48 hours. The concentration of ANP protein in the culture medium was measured using an enzyme-linked immunoassay kit (Phoenix Pharmaceuticals).

Analysis of expression of alternatively spliced Igf1 mRNA. IGF-1 is controlled by 2 distinct promoters associated with untranslated exons 1 and 2, which generate two types of mRNA, containing either exon 1 (class 1 mRNA) or exon 2 (class 2 mRNA) plus a common block of translated exons (53–55). Expression of the two transcripts is differentially regulated in different tissues and species and during development. We therefore determined which mRNA was the major transcript in mouse heart. The respective abundances of the two transcripts were analyzed using real-time PCR with primer sets that specifically amplified either the class 1 or class 2 mRNA. To calculate absolute numbers of transcripts in a given amount of total RNA, we used external standards containing known numbers of class 1 or 2 cDNA fragments. We found that class 2 transcripts were much more abundant in both cardiac fibroblasts and cardiomyocytes than class 1 transcripts, and also in hearts after LI-TAC (Supplemental Figure 17). We therefore analyzed expression of class 2 mRNA as the major *Igf1* transcript in the heart and cardiac fibroblasts (Figure 6, A–C). *Igf1* class 1 and class 2 cDNA fragments were amplified using a forward primer specific for each leader exon (exon 1, 5′-ATGGGGAAAATCAGCAGTC-3′; exon 2, 5′-CTGCCTGTGTAAACGACCCGG-3′) and a reverse primer (exon 3-4 junction, 5′-GGCTGCTTTTGTAGGCTTCAGTGG-3′) (56).

Igf1 promoter–luciferase constructs. Because the class 2 *Igf1* mRNA is much more abundantly expressed than class 1 mRNA in the heart, we analyzed

the promoter associated with exon 2 (33). A genomic fragment of the 5′-flanking region and a part of exon 2 (–80 to +43 bp) was obtained by PCR using mouse genomic DNA. The promoter fragment was then subcloned into a pGL3 basic luciferase reporter vector (Promega) to generate pGL3-*Igf1*. A mutation within the potential KLF-binding motif was introduced by PCR to generate pGL3-*igf1*mutKLF. NIH-3T3 cells grown to 60%–80% confluence were then transfected with the vectors, after which luciferase activities were measured and normalized to β-galactosidase activity. The *Klf5* expression vector was described previously (57). The *Klf15* expression vector was obtained by inserting the *Klf15* cDNA into pCAGMS (14).

ChIP. ChIP assays were performed as previously described (29, 58). Mouse cardiac fibroblasts were formalin fixed, and then chromatin samples were immunoprecipitated using anti-KLF5 mouse monoclonal antibody (KM3918) or control IgG antibody. PCR was performed with the following region-specific primers: for the mouse *Igf1* KLF5 site within the exon 2–associated promoter, 5′-ACCCAGGCTCAGAGCATACC-3′ and 5′-GGGTCGTTTACACAGCAGGT-3′; for intron 2 (an intronic region +750 bp from the translation initiation site that does not contain KLF-binding motifs; negative control), 5′-CCTTCACCGCTCTCTGAAAC-3′ and 5′-CATCAGGGCTTCATGGTTCT-3′; and for the *Pdgfa* KLF5 site, 5′-ATGTAGCTGCCTGCGTGAG-3′ and 5′-CGACAGGGAGGGGGTTATAG-3′.

Statistics. Data are shown as mean ± SEM. Paired data were evaluated using Student's *t* test. Comparisons between multiple groups were made using 1-way ANOVA followed by a post-hoc Bonferroni test. Survival rates among mice were analyzed using long-rank test. *P* values less than 0.05 were considered statistically significant.

Acknowledgments

We thank N. Yamanaka, Y. Xiao, A. Ono, M. Hayashi, and E. Magoshi for their excellent technical assistance. This study was supported by Grants-in-Aid for Scientific Research (to N. Takeda, I. Manabe, R. Nagai) and a grant for Translational Systems Biology and Medicine Initiative from the Ministry of Education, Culture, Sports, Science and Technology of Japan; a research grant from the National Institute of Biomedical Innovation (to R. Nagai); and a research grant from the Japan Science and Technology Institute (to I. Manabe). P. Snider is supported by NIH T32 HL079995 Training Grant in Vascular Biology and Medicine, and S.J. Conway is partially supported by the Riley Children's Foundation and the NIH.

Received for publication June 24, 2009, and accepted in revised form October 21, 2009.

Address correspondence to: Ryozo Nagai or Ichiro Manabe, Department of Cardiovascular Medicine, University of Tokyo Graduate School of Medicine, 7-3-1 Hongo, Bunkyo, Tokyo 113-8655, Japan. Phone: 81-3-5800-6526; Fax: 81-3-3818-6673; E-mail: nagai-tky@umin.ac.jp (R. Nagai); manabe-tky@umin.ac.jp (I. Manabe).

1. Frey N, Olson EN. Cardiac hypertrophy: the good, the bad, and the ugly. *Annu Rev Physiol.* 2003;65:45–79.
2. Baudino TA, Carver W, Giles W, Borg TK. Cardiac fibroblasts: friend or foe? *Am J Physiol Heart Circ Physiol.* 2006;291(3):H1015–H1026.
3. Manabe I, Shindo T, Nagai R. Gene expression in fibroblasts and fibrosis: involvement in cardiac hypertrophy. *Circ Res.* 2002;91(12):1103–1113.
4. Eghbali M, et al. Collagen chain mRNAs in isolated heart cells from young and adult rats. *J Mol Cell Cardiol.* 1988;20(3):267–276.
5. Zak R. Cell proliferation during cardiac growth. *Am J Cardiol.* 1973;31(2):211–219.
6. Kuwahara K, et al. Involvement of cardiotrophin-1 in cardiac myocyte-nonmyocyte interactions during hypertrophy of rat cardiac myocytes in vitro. *Circulation.* 1999;100(10):1116–1124.
7. Harada M, et al. Significance of ventricular myocytes and nonmyocytes interaction during cardiocyte hypertrophy: evidence for endothelin-1 as a paracrine hypertrophic factor from cardiac nonmyocytes. *Circulation.* 1997;96(10):3737–3744.
8. Sano M, et al. Interleukin-6 family of cytokines mediate angiotensin II-induced cardiac hypertrophy in rodent cardiomyocytes. *J Biol Chem.* 2000;275(38):29717–29723.
9. Oka T, et al. Genetic manipulation of periostin expression reveals a role in cardiac hypertrophy and ventricular remodeling. *Circ Res.* 2007;101(3):313–321.
10. King KL, et al. Phenylephrine, endothelin, prostaglandin F2alpha' and leukemia inhibitory factor induce different cardiac hypertrophy phenotypes in vitro. *Endocrine.* 1998;9(1):45–55.
11. Ieda M, et al. Cardiac fibroblasts regulate myocardial proliferation through beta1 integrin signaling. *Dev Cell.* 2009;16(2):233–244.
12. Thum T, et al. MicroRNA-21 contributes to myocardial disease by stimulating MAP kinase signalling in fibroblasts. *Nature.* 2008;456(7224):980–984.
13. Haldar SM, Ibrahim OA, Jain MK. Kruppel-like Factors (KLFs) in muscle biology. *J Mol Cell Cardiol.* 2007;43(1):1–10.
14. Shindo T, et al. Kruppel-like zinc-finger transcription factor KLF5/BTEB2 is a target for angiotensin II signaling and an essential regulator of cardiovascular remodeling. *Nat Med.* 2002;8(8):856–863.
15. Nagai R, Suzuki T, Aizawa K, Shindo T, Manabe I. Significance of the transcription factor KLF5 in cardiovascular remodeling. *J Thromb Haemost.* 2005;3(8):1569–1576.
16. Forsberg K, Valyi-Nagy I, Heldin CH, Herlyn M, Westermark B. Platelet-derived growth factor (PDGF) in oncogenesis: development of a vascular connective tissue stroma in xenotransplanted human melanoma producing PDGF-BB. *Proc Natl Acad Sci U S A.* 1993;90(2):393–397.
17. Lindahl P, Johansson BR, Leveen P, Betsholtz C. Pericyte loss and microaneurysm formation in PDGF-B-deficient mice. *Science.* 1997;277(5323):242–245.
18. Raines EW. PDGF and cardiovascular disease. *Cytokine Growth Factor Rev.* 2004;15(4):237–254.
19. Andrae J, Gallini R, Betsholtz C. Role of platelet-derived growth factors in physiology and medicine. *Genes Dev.* 2008;22(10):1276–1312.
20. Agah R, et al. Gene recombination in postmitotic cells. Targeted expression of Cre recombinase provokes cardiac-restricted, site-specific rearrangement in adult ventricular muscle in vivo. *J Clin Invest.* 1997;100(1):169–179.
21. Lindsley A, et al. Identification and characterization of a novel Schwann and outflow tract endocardial cushion lineage-restricted periostin enhancer. *Dev Biol.* 2007;307(2):340–355.
22. Joseph NM, et al. The loss of Nf1 transiently promotes self-renewal but not tumorigenesis by neural crest stem cells. *Cancer Cell.* 2008;13(2):129–140.
23. Conway SJ, Molkentin JD. Periostin as a Heterofunctional Regulator of Cardiac Development and Disease. *Current Genomics.* 2008;9(8):548–555.
24. Snider P, et al. Periostin is required for maturation and extracellular matrix stabilization of noncardiomyocyte lineages of the heart. *Circ Res.* 2008;102(7):752–760.
25. Dorn GW, 2nd. Periostin and myocardial repair, regeneration, and recovery. *N Engl J Med.* 2007;357(15):1552–1554.
26. Soriano P. Generalized lacZ expression with the ROSA26 Cre reporter strain. *Nat Genet.* 1999;21(1):70–71.
27. Shioya T. A simple technique for isolating healthy heart cells from mouse models. *J Physiol Sci.* 2007;57(6):327–335.
28. Hudon-David F, Bouzeghrane F, Couture P, Thibault G. Thy-1 expression by cardiac fibroblasts: lack of association with myofibroblast contractile markers. *J Mol Cell Cardiol.* 2007;42(5):991–1000.
29. Oishi Y, et al. SUMOylation of Kruppel-like transcription factor 5 acts as a molecular switch in transcriptional programs of lipid metabolism involving PPAR-delta. *Nat Med.* 2008;14(6):656–666.
30. Serose A, Salmon A, Fiszman MY, Fromes Y. Short-term treatment using insulin-like growth factor-1 (IGF-1) improves life expectancy of the delta-sarcoglycan deficient hamster. *J Gene Med.* 2006;8(8):1048–1055.
31. Abbas A, Grant PJ, Kearney MT. Role of IGF-1 in glucose regulation and cardiovascular disease. *Expert Rev Cardiovasc Ther.* 2008;6(8):1135–1149.
32. McMullen JR. Role of insulin-like growth factor 1 and phosphoinositide 3-kinase in a setting of heart disease. *Clin Exp Pharmacol Physiol.* 2008;35(3):349–354.
33. Wang X, Talamantez JL, Adamo ML. A CACCC box in the proximal exon 2 promoter of the rat insulin-like growth factor I gene is required for basal promoter activity. *Endocrinology.* 1998;139(3):1054–1066.
34. Wang B, et al. The Kruppel-like factor KLF15 inhibits connective tissue growth factor (CTGF) expression in cardiac fibroblasts. *J Mol Cell Cardiol.* 2008;45(2):193–197.
35. Fisch S, et al. Kruppel-like factor 15 is a regulator of cardiomyocyte hypertrophy. *Proc Natl Acad Sci U S A.* 2007;104(17):7074–7079.
36. Ema M, et al. Kruppel-like factor 5 is essential for blastocyst development and the normal self-renewal of mouse ESCs. *Cell Stem Cell.* 2008;3(5):555–567.
37. Parisi S, et al. Klf5 is involved in self-renewal of mouse embryonic stem cells. *J Cell Sci.* 2008;121(Pt 16):2629–2634.
38. Jiang J, et al. A core Klf circuitry regulates self-renewal of embryonic stem cells. *Nat Cell Biol.* 2008;10(3):353–360.
39. Aizawa K, et al. Regulation of platelet-derived growth factor-A chain by Kruppel-like factor 5: new pathway of cooperative activation with nuclear factor-kappaB. *J Biol Chem.* 2004;279(1):70–76.
40. Pietrzkowski Z, Wernicke D, Porcu P, Jameson BA, Baserga R. Inhibition of cellular proliferation by

peptide analogues of insulin-like growth factor 1. *Cancer Res.* 1992;52(23):6447–6451.
41. Sano M, et al. p53-induced inhibition of Hif-1 causes cardiac dysfunction during pressure overload. *Nature.* 2007;446(7134):444–448.
42. Welch S, et al. Cardiac-specific IGF-1 expression attenuates dilated cardiomyopathy in tropomodulin-overexpressing transgenic mice. *Circ Res.* 2002;90(6):641–648.
43. Li B, et al. Insulin-like growth factor-1 attenuates the detrimental impact of nonocclusive coronary artery constriction on the heart. *Circ Res.* 1999;84(9):1007–1019.
44. Kajstura J, et al. IGF-1 overexpression inhibits the development of diabetic cardiomyopathy and angiotensin II-mediated oxidative stress. *Diabetes.* 2001;50(6):1414–1424.
45. Li Q, et al. Overexpression of insulin-like growth factor-1 in mice protects from myocyte death after infarction, attenuating ventricular dilation, wall stress, and cardiac hypertrophy. *J Clin Invest.* 1997;100(8):1991–1999.
46. McMullen JR, et al. The insulin-like growth factor 1 receptor induces physiological heart growth via the phosphoinositide 3-kinase(p110alpha) pathway. *J Biol Chem.* 2004;279(6):4782–4793.
47. Lavallee G, et al. The Kruppel-like transcription factor KLF13 is a novel regulator of heart development. *EMBO J.* 2006;25(21):5201–5213.
48. Subramaniam M, Hawse JR, Johnsen SA, Spelsberg TC. Role of TIEG1 in biological processes and disease states. *J Cell Biochem.* 2007;102(3):539–548.
49. Wakeland E, Morel L, Achey K, Yui M, Longmate J. Speed congenics: a classic technique in the fast lane (relatively speaking). *Immunol Today.* 1997;18(10):472–477.
50. Rockman HA, et al. Segregation of atrial-specific and inducible expression of an atrial natriuretic factor transgene in an in vivo murine model of cardiac hypertrophy. *Proc Natl Acad Sci U S A.* 1991;88(18):8277–8281.
51. Komuro I, et al. Isolation and characterization of two isozymes of myosin heavy chain from canine atrium. *J Biol Chem.* 1986;261(10):4504–4509.
52. Komuro I, et al. Stretching cardiac myocytes stimulates protooncogene expression. *J Biol Chem.* 1990;265(7):3595–3598.
53. Lin WW, Oberbauer AM. Alternative splicing of insulin-like growth factor I mRNA is developmentally regulated in the rat and mouse with preferential exon 2 usage in the mouse. *Growth Horm IGF Res.* 1998;8(3):225–233.
54. Shemer J, Adamo ML, Roberts CT Jr, LeRoith, D. Tissue-specific transcription start site usage in the leader exons of the rat insulin-like growth factor-I gene: evidence for differential regulation in the developing kidney. *Endocrinology.* 1992; 131(6):2793–2799.
55. O'Sullivan DC, Szestak TA, Pell JM. Regulation of IGF-I mRNA by GH: putative functions for class 1 and 2 message. *Am J Physiol Endocrinol Metab.* 2002:283(2):E251–E258.
56. Ohtsuki T, Otsuki M. Murakami Y, Hirata K, Takeuchi S, Takahashi S. Alternative leader-exon usage in mouse IGF-I mRNA variants: class 1 and class 2 IGF-I mRNAs. *Zoolog Sci.* 2007;24(3):241–247.
57. Oishi Y, et al. Kruppel-like transcription factor KLF5 is a key regulator of adipocyte differentiation. *Cell Metab.* 2005;1(1):27–39.
58. Manabe I, Owens GK. CArG elements control smooth muscle subtype-specific expression of smooth muscle myosin in vivo. *J Clin Invest.* 2001;107(7):823–834.

Persistent Cardiac Aldosterone Synthesis in Angiotensin II Type 1A Receptor–Knockout Mice After Myocardial Infarction

Jun Katada, PhD; Tomomi Meguro, MD; Hitomi Saito, BSc; Akira Ohashi, MD; Toshihisa Anzai, MD; Satoshi Ogawa, MD; Tsutomu Yoshikawa, MD

Background—The renin-angiotensin-aldosterone system is implicated in the pathogenesis of heart failure. Pharmacological blockade of angiotensin II (Ang II)–dependent signaling is clinically effective in reducing cardiovascular events after myocardial infarction (MI) but still fails to completely prevent remodeling. The molecular basis underlying this Ang II–independent remodeling is unclear.

Methods and Results—Acute MI was induced by coronary ligation in wild-type (WT) and angiotensin II type IA receptor–knockout (AT_{1A}-KO) mice. Left ventricular (LV) geometry, hemodynamics, and cardiac gene expression were evaluated on day 28. Severe LV remodeling and resultant cardiac dysfunction were observed in WT mice, whereas less marked, but still significant, LV remodeling and cardiac dysfunction were induced in AT_{1A}-KO mice. Gene expression levels of aldosterone synthase and the cardiac aldosterone content were both elevated in the MI hearts, even in AT_{1A}-KO mice. In AT_{1A}-KO mice treated with spironolactone (20 mg/kg per day), LV remodeling, cardiac dysfunction, and cardiac gene expression of collagens and natriuretic peptides were almost normalized.

Conclusions—Our results indicate that genetic blockade of AT_{1A} signaling fails to arrest aldosterone production in cardiac tissues and that cardiac aldosterone plays a critical role in post-MI LV remodeling. The results suggest that spironolactone could be potentially effective in patients with MI, when used in combination with renin-angiotensin system blockade, by blocking the actions of aldosterone produced by Ang II–independent mechanisms. (***Circulation.* 2005;111:2157-2164.**)

Key Words: myocardial infarction ■ remodeling ■ angiotensin

The renin-angiotensin-aldosterone system is closely involved in the pathogenesis of heart failure. Previous studies have shown that angiotensin-converting enzyme (ACE) inhibitors and angiotensin II (Ang II) receptor blockers reduce mortality and morbidity among patients with chronic heart failure (CHF) and left ventricular (LV) systolic dysfunction.[1,2] However, cardiac dysfunction and cardiovascular deaths are still observed even when CHF patients are treated with ACE inhibitors or Ang II receptor blockers. The aldosterone escape phenomenon, ie, persistent production of aldosterone despite renin-angiotensin system blockade, may be responsible for the insufficient action of ACE inhibitors or Ang II receptor blockers in patients with CHF.

In the Randomized Aldactone Evaluation Study (RALES), treatment with the mineralocorticoid receptor antagonist spironolactone reduced overall mortality in patients with advanced heart failure.[3] This finding was recently confirmed by The Eplerenone Postacute Myocardial Infarction Heart Failure Efficacy and Survival Study (EPHESUS) in postinfarction CHF patients with the use of a new selective mineralocorticoid receptor antagonist, eplerenone.[4] It has also been reported that mineralocorticoid receptor antagonists prevent LV dysfunction and remodeling in several animal models of heart failure.[5,6] Although one of the primary targets of aldosterone is the kidney, there is also evidence that aldosterone directly affects cardiac tissues and causes the development of cardiac hypertrophy, fibrosis, and heart failure.[7,8]

Accumulating evidence suggests production of aldosterone in cardiac tissues, particularly under pathological conditions. Aldosterone synthase (CYP11B2) is detected in the hearts of several species, including rats[9,10] and humans.[11,12] Cardiac aldosterone production has also been found in experiments demonstrating a gradient of plasma aldosterone concentrations between the anterior interventricular vein and coronary sinus in humans,[13,14] and myocardial production of aldosterone has been demonstrated in the rat.[15] Increased production of cardiac aldosterone under certain pathological conditions suggests that it could play an important role in the pathogenesis of cardiac diseases. However, there is little or no information on the regulation of cardiac synthesis of aldosterone apart from the finding of involvement of the local renin-angiotensin system.[16]

Received July 2, 2004; revision received December 16, 2004; accepted December 21, 2004.

From the Pfizer-KEIO Research Laboratory (J.K., T.M., H.S., A.O.) and Cardiopulmonary Division, Keio University School of Medicine (S.O., T.A., T.Y.), Tokyo, Japan.

Correspondence to Jun Katada, PhD, Research Park 2N4, Keio University School of Medicine, Shinanomachi 35, Shinjuku-ku, Tokyo 160-8582, Japan. E-mail katada@kt.rim.or.jp

Circulation **is available at http://www.circulationaha.org** **DOI: 10.1161/01.CIR.0000163562.82134.8E**

Harada et al[17] demonstrated that Ang II type 1A receptor (AT_{1A}) signals play a pivotal role in the progression of post–myocardial infarction (MI) LV remodeling, using genetically AT_{1A}-deficient (knockout) (AT_{1A}-KO) mice. However, it is notable that LV remodeling and cardiac dysfunction still occurred, even after AT_{1A}-dependent signaling was eliminated completely. Hence, we hypothesized that Ang II–independent synthesis of cardiac aldosterone in post-MI hearts may be responsible for persistent LV remodeling. The aims of the present study were to determine whether Ang II–independent aldosterone synthesis is induced in the hearts of AT_{1A}-KO mice after acute MI and to elucidate the pathophysiological roles of cardiac aldosterone synthesis in post-MI remodeling.

Methods

Animals

Male 15-week-old AT_{1A}-KO mice (n=40) were used in the study.[18] Age-matched male mice with the same genetic background (wild-type [WT]) were used as controls (n=40). All experimental protocols conformed to international guidelines and were approved by the animal experimentation review board of Keio University School of Medicine.

Induction of MI

MI was induced with the coronary ligation technique, as described previously.[17] Sham-operated mice were prepared in the same manner, but no coronary ligation was performed. Spironolactone (Sigma) was administered orally at 20 mg/kg per day for 28 days. Lisinopril was administered for 28 days by mixing with drinking water. The estimated dose of lisinopril was 20 mg/kg per day, which has been reported to prevent LV fibrosis in rats.[19]

Evaluation of Infarcted Hearts at Day 28

Echocardiography was performed in mice anesthetized with ketamine (70 mg/kg IP) and xylazine (4 mg/kg IP) with the use of an ultrasonograph (EnVisor, Philips Medical Systems Japan) equipped with a dynamically focused 9-MHz annular array transducer, as described previously.[20] Hemodynamics were assessed with a 1.4F high-fidelity catheter (Millar Instruments Inc) inserted via the right carotid artery into the LV for recording LV systolic pressure, heart rate, and maximal rate of rise of LV pressure (dP/dT_{max}). Finally, the hearts were excised, and the LV with scar and the right ventricle (RV) were weighed separately. Evaluation of the infarct size, expressed as a percentage of the LV surface area, was conducted as described previously[21] with the use of formalin-fixed longitudinal sections of LV. Hydroxyproline contents, a marker for the cardiac collagen protein level, were determined as described previously.[22]

Quantitative Reverse Transcription–Polymerase Chain Reaction

For quantitative reverse transcription–polymerase chain reaction (RT-PCR), total RNA, extracted from noninfarcted LV walls, was reverse transcribed to cDNA with $oligo(dT)_{16}$ primers. PCR reactions were performed with the ABI PRISM 7700 Sequence Detector System (Applied Biosystems), which monitors the PCR reaction in real time. Oligonucleotide primers and TaqMan probes were designed from the GenBank databases with the use of Primer Express software (Applied Biosystems).[23] Statistical analysis of the results was performed with the ΔCt value ($Ct_{gene\ of\ interest} - Ct_{GAPDH}$). Relative gene expression was obtained by ΔΔCt methods (ΔCt sample − ΔCt calibrator), with WT sham mice used for comparison with the gene expression level of unknown samples.

Biochemical Analyses

Cardiac aldosterone was extracted from the hearts as described previously.[15] Briefly, the excised hearts were washed thoroughly with ice-cold PBS to remove blood and then homogenized in 1 mL of methanol with the use of a Polytron homogenizer. After centrifugation at 3000*g* for 15 minutes, the supernatant was dried under vacuum (Savant Speed Vac SC-100 system) and then mixed with 1 mL PBS. Aldosterone concentrations were determined by radioimmunoassay system. Tissue aldosterone levels were expressed in pg/mg protein. Plasma aldosterone was directly determined by radioimmunoassay. Sodium and potassium concentrations in plasma samples, prepared from blood collected from the right carotid artery in chilled tubes containing 2 μL EDTA, were determined by flame photometry. Plasma concentrations of corticotropin were determined by radioimmunoassay.[24]

Statistical Analysis

All data are expressed as mean±SEM. Multiple comparisons were performed by 1-way ANOVA with Bonferroni correction. A probability value <0.05 was considered statistically significant.

Results

Mortality Rate After Induction of MI

Eight of 40 WT MI mice died during the 28-day observation period (mortality rate, 20%). The mortality rate by day 28 was significantly lower in WT MI mice treated with spironolactone (7.5%) and in AT_{1A}-KO MI mice (10%) than in untreated WT MI mice. All spironolactone-treated AT_{1A}-KO MI mice and sham-operated mice survived throughout the experiment.

Body Weight, Infarct Size, and Tissue Weight

The percent infarct area was not statistically different among the 4 MI groups (vehicle-treated WT: 37±0.9%; vehicle-treated AT_{1A}-KO: 37±0.9%; spironolactone-treated WT: 36±0.9%; spironolactone-treated AT_{1A}-KO: 37±0.9%). There was no significant difference in body weight on day 28 among the 8 experimental groups (Table). The LV and RV weights of WT MI mice on day 28 were significantly higher than those of WT sham-operated mice (77% and 137% increase for LV and RV, respectively). LV and RV weights of AT_{1A}-KO MI mice were lower than those of WT MI mice but still significantly higher than those of sham-operated AT_{1A}-KO mice. LV and RV weights were further decreased by administration of spironolactone, and consequently these weights in spironolactone-treated AT_{1A}-KO MI mice were comparable to those of sham-operated mice. Changes in lung weight showed similar trends.

Echocardiographic Study

As shown in Figure 1A, LV posterior wall thickness was increased by 67.6% in WT MI mice compared with WT sham-operated mice. LV posterior wall thickness was also thicker in AT_{1A}-KO mice, but a smaller increase in thickness occurred compared with that in AT_{1A}-KO sham-operated mice. When given to AT_{1A}-KO mice, spironolactone induced a further reduction in LV posterior wall thickness and almost normalized the wall thickness after MI. Similarly, LV end-diastolic internal diameter and LV systolic internal diameter were higher in WT MI mice than WT sham-operated mice (47% and 149% increase, respectively). Both changes were attenuated in AT_{1A}-KO MI mice (Figure 1B and 1C), although both diameters were still

Body, Heart, and Lung Weight in Mice With MI

Conditions	Body Weight	LV Weight	RV Weight	Lung Weight
WT/MI/vehicle	29.0±0.36	155.7±4.29*	51.7±3.36*	207.1±8.19*
KO/MI/vehicle	30.1±0.31	107.1±4.19*†	31.6±3.02*†	184.7±11.3*†
WT/MI/spironolactone	29.3±0.26	106.6±2.88*†	28.5±1.75*†	151.5±2.47†
KO/MI/spironolactone	30.1±0.63	92.1±3.33†	25.7±2.19†	164.0±3.47†
WT/sham/vehicle	28.8±0.59	87.9±1.95	21.8±1.14	152.1±5.05
KO/sham/vehicle	30.2±1.03	85.6±4.38	22.8±0.86	155.8±7.40
WT/sham/spironolactone	29.4±0.65	87.3±3.03	21.0±1.13	152.0±4.97
KO/sham/spironolactone	30.4±0.63	86.0±5.52	20.5±2.33	151.3±6.25

WT indicates wild-type mice; KO, AT_{1A}-knockout mice; MI, mice with myocardial infarction; sham, sham-operated mice; spironolactone, spironolactone-treated mice; and vehicle, vehicle-treated mice. Spironolactone-treated mice were treated with spironolactone (20 mg/kg per day PO) for 4 weeks, and vehicle-treated mice were treated with vehicle (0.5% methylcellulose) alone.

*$P<0.05$ compared with sham-operated control mice; †$P<0.05$ compared with vehicle-treated MI WT mice.

larger than those of AT_{1A}-KO sham-operated mice. In spironolactone-treated AT_{1A}-KO MI mice, further inhibition of LV dimensions was observed. Consequently, percent fractional shortening value was significantly higher in spironolactone-treated AT_{1A}-KO MI mice than in vehicle-treated AT_{1A}-KO MI mice (Figure 1D).

Spironolactone Improves Impaired Cardiac Function

As shown in Figure 2A, LV systolic pressure was decreased by 27.3% in WT MI mice (92.2±3.0 mm Hg in WT sham mice versus 67.0±2.4 mm Hg in WT MI mice; $P<0.01$). The decrease in LV systolic pressure was much smaller in AT_{1A}-KO mice (10.3% decrease compared with sham

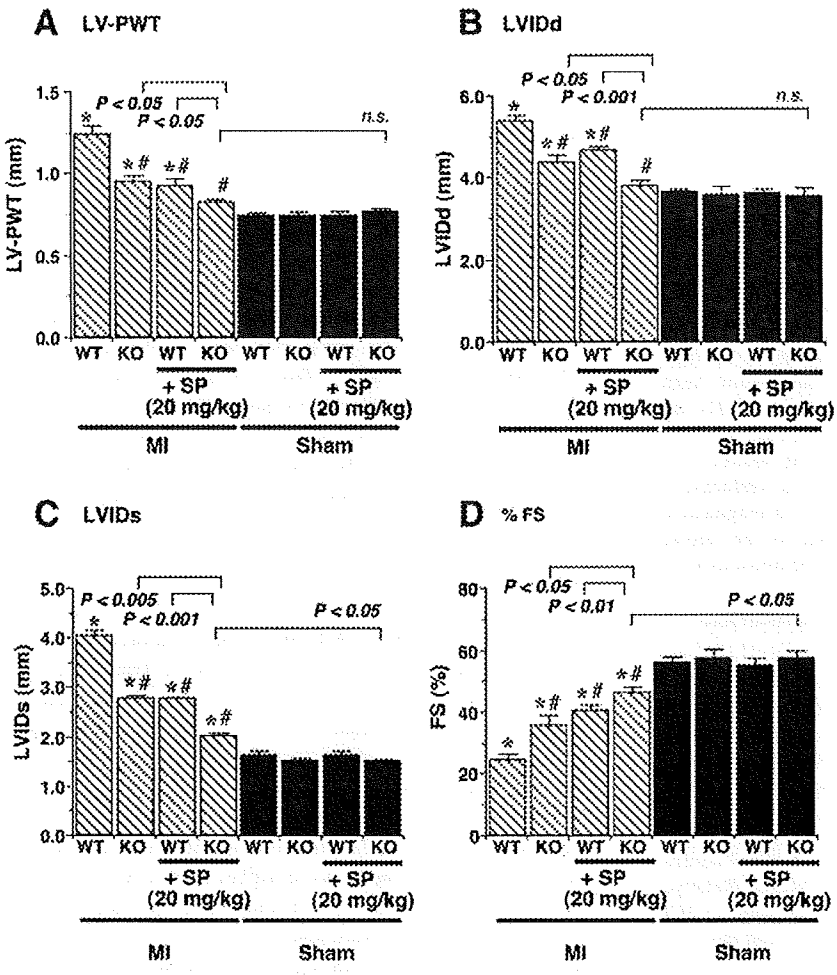

Figure 1. LV posterior wall thickness (LV-PWT) (A), end-diastolic left ventricular internal diameter (LVIDd) (B), end-systolic left ventricular internal diameter (LVIDs) (C), and fractional shortening (%FS) (D) 28 days after MI. KO indicates AT_{1A}-knockout mice; SP, treatment with spironolactone. Data are mean±SEM of 5 to 10 mice. *$P<0.05$ compared with sham-operated control mice; #$P<0.05$ compared with vehicle-treated MI WT mice.

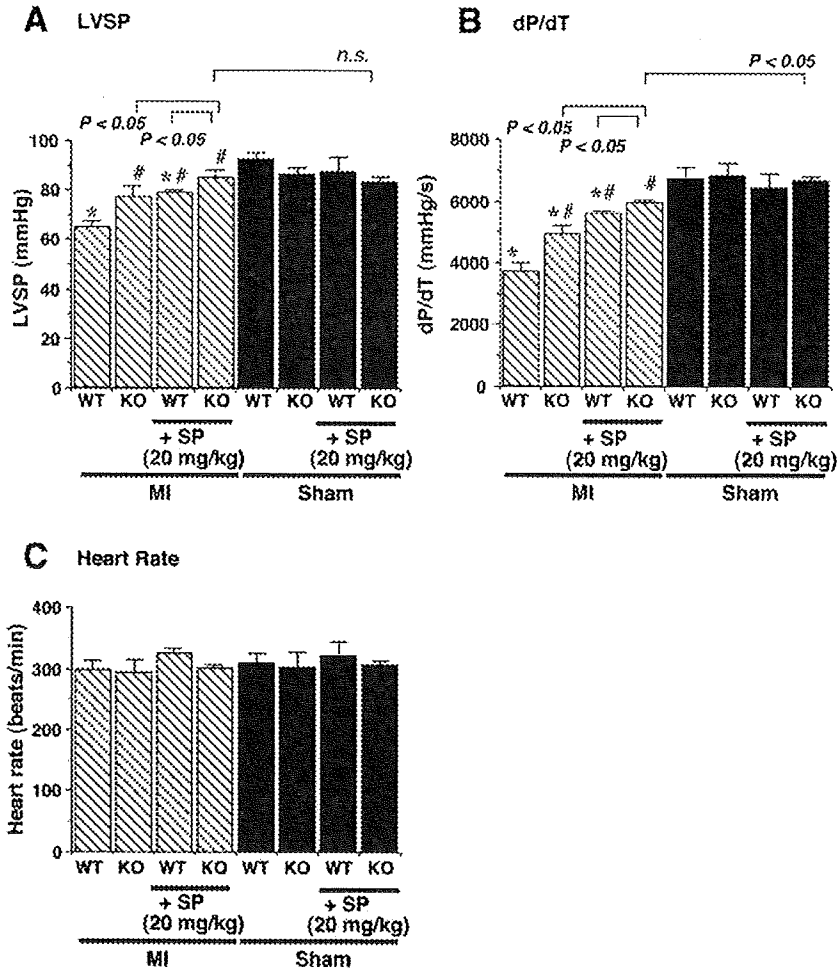

Figure 2. LV systolic pressure (LVSP) (A), dP/dT_{max} (B), and heart rate (C) 28 days after MI. KO indicates AT_{1A}-knockout mice; SP, treatment with spironolactone. Data are mean±SEM of 5 to 10 mice. *$P<0.05$ compared with sham-operated control mice; #$P<0.05$ compared with vehicle-treated MI WT mice.

AT_{1A}-KO mice). Administration of spironolactone to AT_{1A}-KO MI mice induced further attenuation of the LV systolic pressure decline, which became close to normal levels. Similar changes were noted in dP/dT (Figure 2B). A large reduction of dP/dT was observed in WT MI mice (45% reduction compared with WT sham mice; $P<0.001$). In contrast, dP/dT decrease was significantly attenuated in AT_{1A}-KO MI mice. Spironolactone reversed the decrease in dP/dT observed in AT_{1A}-KO MI mice. The heart rate was not statistically different among the 8 experimental groups (Figure 2C).

Gene Expression and Collagen Level in Noninfarcted LV

As shown in Figure 3A and 3B, the expression levels of atrial natriuretic peptide (ANP) and B-type natriuretic peptide (BNP) mRNAs, which are markers of cardiac hypertrophy, were enhanced in WT MI mice compared with WT sham mice (ANP: 6.3±0.4-fold increase; BNP: 4.9±0.4-fold increase). Upregulation of mRNA expression of both ANP and BNP was also observed in AT_{1A}-KO MI mice, but the expression levels were significantly lower than those in WT MI mice. Further inhibition of ANP and BNP mRNA expression was noted when AT_{1A}-KO MI mice were treated with spironolactone, resulting in the expression levels being almost comparable to those of sham-operated mice. As shown in Figure 3C and 3D, the expression levels of type I and type III collagen genes were higher in WT MI mice than in WT sham mice (type I collagen: 16.3±0.7-fold increase; type III collagen: 14.4±0.7-fold increase). Upregulation of these genes was partially attenuated in AT_{1A}-KO MI mice. Treatment of AT_{1A}-KO MI mice with spironolactone further attenuated the expression levels. Hydroxyproline content in the LV wall, a marker for collagen proteins, exhibited a similar trend (Figure 3E).

Cardiac Production of Aldosterone

Quantitative RT-PCR showed small but detectable levels of CYP11B2 mRNA in sham-operated hearts. As shown in Figure 4A, the CYP11B2 expression level was significantly higher in WT MI hearts than in sham-operated mice (5.4±0.6-fold increase; $P<0.01$). In AT_{1A}-KO MI mice, CYP11B2 gene expression was lower than in WT MI mice but still was significantly higher than in sham-operated AT_{1A}-KO mice. CYP11B2 gene expression in adrenal gland did not differ in WT and KO mice with or without MI (data not shown).

The cardiac aldosterone level was elevated in MI mice (Figure 4B) (297±40.3 pg/mg protein in WT MI mice versus 68±5.6 pg/mg protein in WT sham mice; $P<0.001$). A

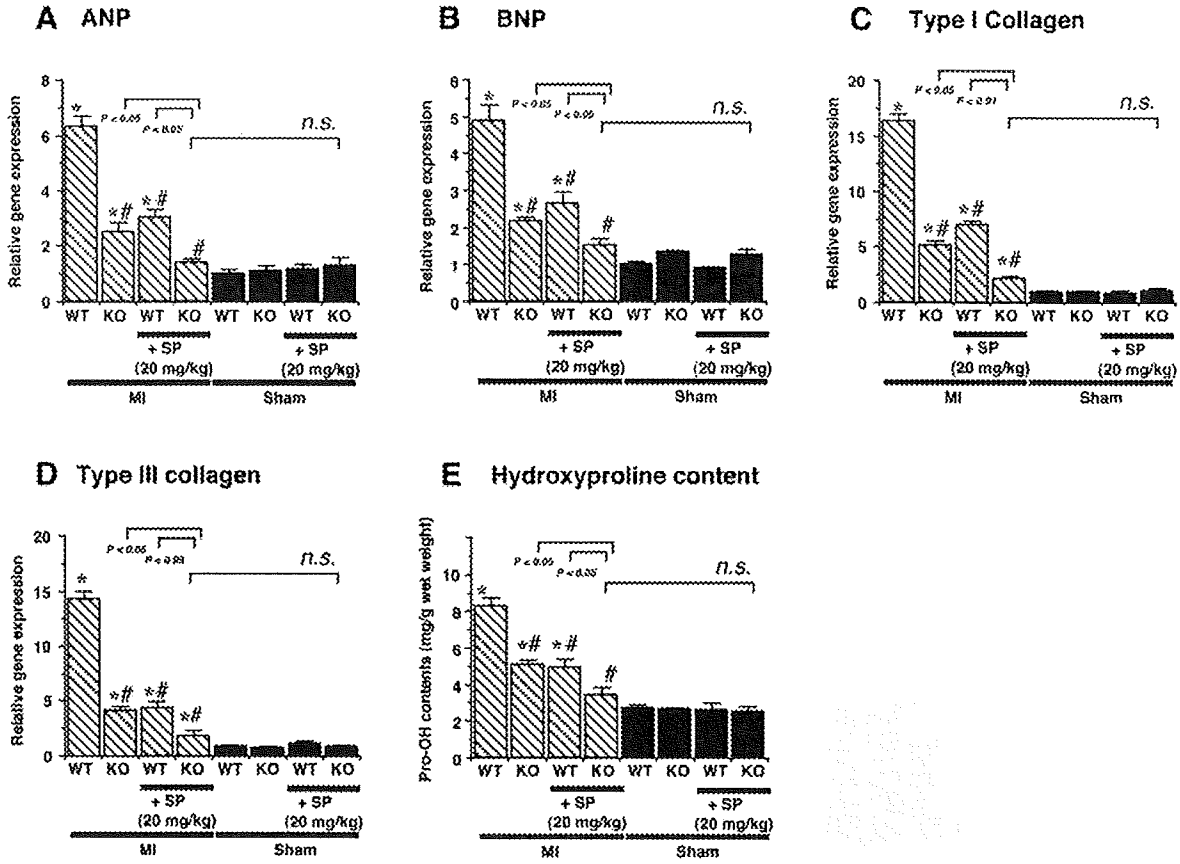

Figure 3. Messenger RNA expression levels of ANP (A), BNP (B), type I collagen (C), and type III collagen (D) in noninfarcted region of LV were determined by quantitative RT-PCR 28 days after MI. Each mRNA level is relative to the expression level of GAPDH gene and presented as a relative value with the WT sham mice used for comparison. E, Hydroxyproline (Pro-OH) content in LV noninfarct area. KO indicates AT_{1A}-knockout mice; SP, treatment with spironolactone. Data are mean±SEM of 5 to 10 mice. *$P<0.05$ compared with sham-operated control mice; #$P<0.05$ compared with vehicle-treated MI WT mice.

significantly high aldosterone level was also observed in AT_{1A}-KO MI mice compared with AT_{1A}-KO sham-operated mice, but the increase was smaller than that in WT MI mice. Plasma aldosterone levels were 0.17±0.02 ng/mL in WT sham-operated mice, 0.25±0.02 ng/mL in WT MI mice ($P<0.05$ versus WT sham mice), 0.16±0.03 ng/mL in AT_{1A}-KO sham-operated mice, and 0.18±0.02 ng/mL in AT_{1A}-KO MI mice (nonsignificant versus AT_{1A}-KO sham-operated mice).

Mechanism Underlying Renin-Angiotensin System–Independent Aldosterone Production

To examine the possible involvement of Ang II or other active products of the renin-angiotensin system, such as

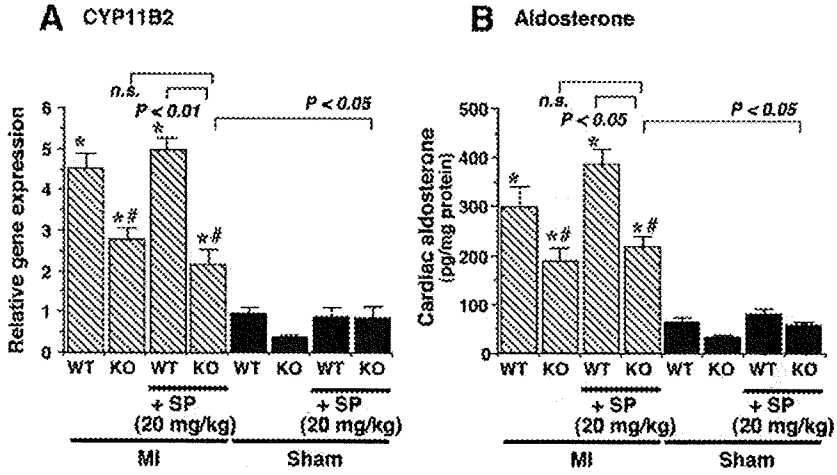

Figure 4. A, CYP 11B2 mRNA levels on day 28 determined by quantitative RT-PCR. The expression level of each sample was expressed relative to the expression level of GAPDH gene and is presented as a relative value with the WT sham mice used as a calibrator for comparison. Data are mean±SEM of 5 to 10 mice. B, Mean±SEM values of aldosterone contents in MI hearts (n=5). KO indicates AT_{1A}-knockout mice; SP, treatment with spironolactone. *$P<0.05$ compared with sham-operated control mice; #$P<0.05$ compared with vehicle-treated WT MI mice.

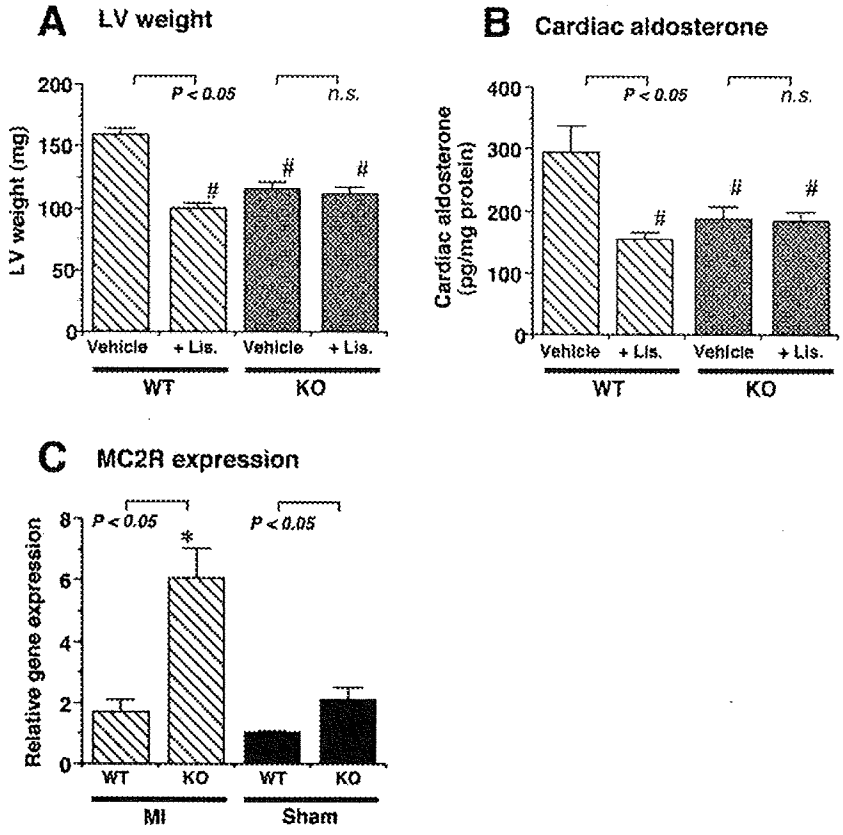

Figure 5. LV weight (A) and cardiac aldosterone levels (B) on day 28 in WT and KO MI mice treated with lisinopril (+Lis., 20 mg/kg per day). C, MC2R mRNA levels at day 28 in noninfarcted LV wall determined by RT-PCR. The expression level of each sample was expressed relative to that of GAPDH gene and is presented as a relative value, with the WT sham mice used for comparison. KO indicates AT_{1A}-knockout mice. *$P<0.05$ compared with sham-operated control mice; #$P<0.05$ compared with vehicle-treated WT MI mice.

Ang_{1-7}, in cardiac aldosterone synthesis through receptors other than AT_{1A}, we examined the effects of lisinopril, an ACE inhibitor. As shown in Figure 5A, treatment with lisinopril (20 mg/kg per day) significantly attenuated LV hypertrophy observed in WT mice but did not further reduce LV weight in AT_{1A}-KO MI mice. Other parameters, including RV weight and the gene expression level of type I collagen, showed similar trends (data not shown). Treatment with lisinopril decreased cardiac aldosterone levels in WT MI mice but not in AT_{1A}-KO MI mice (Figure 5B).

Plasma concentrations of sodium, potassium, and corticotropin on day 28 did not differ among the 8 experimental groups (data not shown). As shown in Figure 5C, gene expression of melanocortin receptor type 2 (MC2R), a corticotropin receptor, was significantly upregulated in the noninfarcted LV wall of AT_{1A}-KO MI mice compared with sham-operated AT_{1A}-KO mice.

Discussion

The major findings of the present study are as follows: (1) AT_{1A}-KO mice with MI had cardiac hypertrophy, cardiac dysfunction, and collagen gene expression, along with increased cardiac expression of the CYP11B2 gene and elevated cardiac aldosterone levels. (2) Spironolactone administration inhibited LV remodeling and resulted in almost normalized LV geometry, as well as reversing altered cardiac gene expressions (ANP, BNP, type I and type III collagens) in AT_{1A}-KO MI mice. These results suggest that aldosterone is produced via an Ang II–independent mechanism in hearts with MI and that it promotes cardiac hypertrophy, fibrosis, and subsequent heart failure after MI.

Several regulators are known to stimulate aldosterone synthesis in the adrenal cortex, including Ang II, corticotropin, and plasma concentrations of Na^+ and/or K^+. Among these, Ang II is the primary physiological regulator because it is well known that blockade of the renin-angiotensin system by ACE inhibitors or Ang II receptor blockers often results in transiently decreased plasma aldosterone concentrations. However, it is also known that the plasma aldosterone concentration returns to a normal or supranormal level after long-term blockade of the renin-angiotensin system, ie, so-called aldosterone escape. The molecular mechanism of this Ang II–independent aldosterone synthesis in adrenal glands has not been clarified to date. In the present study we found that similar Ang II–independent aldosterone synthesis occurs in post-MI hearts. As shown in Figures 4 and 5, cardiac aldosterone content and gene expression of cardiac CYP11B2 were significantly elevated after MI in the hearts of AT_{1A}-KO mice and in WT mice treated with lisinopril compared with the hearts of sham-operated mice. These results suggest that Ang II–independent aldosterone synthesis is induced in post-MI hearts. We confirmed that the plasma aldosterone concentration and CYP11B2 gene expression in the adrenal gland were not changed at this time point (28 days after induction of MI). A previous report has also shown that the cardiac, and not the adrenal, steroidogenic system is activated in MI rats.[9] These data are consistent with results from human clinical studies[25,26] showing that plasma aldosterone concen-

trations were normal or decreased 1 month after the onset of renin-angiotensin system blockade and that the aldosterone escape phenomenon is generally induced only after long-term (several months or longer) treatment. Therefore, it is possible that different molecular mechanisms underlie the aldosterone escape phenomenon in adrenal glands and Ang II–independent aldosterone synthesis in post-MI hearts.

The factors responsible for Ang II–independent aldosterone synthesis are not clear. Our results suggest that a steroidogenic corticotropin receptor, MC2R, may be involved in cardiac Ang II–independent aldosterone synthesis because MC2R receptor expression was significantly upregulated in post-MI hearts in AT_{1A}-KO mice (Figure 5C). MC2R-dependent signaling by corticotropin is known to upregulate a series of steroidogenic enzymes, including CYP11B2. Therefore, it is possible that increased expression of MC2R may be involved in the activation of cardiac aldosterone production via upregulation of steroidogenic enzymes, including CYP11B2, via a renin-angiotensin system–independent mechanism. On the other hand, this pathway does not seem to be activated in the adrenal cortex under our experimental conditions. We detected neither an increased plasma corticotropin concentration nor increased gene expression of MC2R and CYP11B2 in adrenal glands in AT_{1A}-KO mice 28 days after MI. Another possibility for the mechanism underlying cardiac Ang II–independent aldosterone production is evident in our previous study,[9] in which it was demonstrated that treatment of rat MI hearts with high-dose spironolactone (80 mg/kg) resulted in increased expression of cardiac CYP11B2 and increased aldosterone levels. Basically, similar results were obtained in the present study, although there are some minor discrepancies that are probably explained by species differences. These results suggest that aldosterone itself could regulate CYP11B2 expression by a feedback mechanism in post-MI hearts. Thus, our current hypothesis regarding Ang II–independent aldosterone synthesis in post-MI hearts is that an activated corticotropin-dependent signal induced by upregulation of the corticotropin receptor is closely involved in aldosterone production, in addition to increased expression of CYP11B2 elicited by aldosterone. Further studies need to be conducted to elucidate the molecular mechanism underlying the cardiac aldosterone escape phenomenon.

The next key question is whether cardiac aldosterone plays a significant role in post-MI cardiac hypertrophy or fibrosis. The critical roles of aldosterone in vascular damage, cardiac hypertrophy, LV remodeling, or heart failure after acute MI have been widely reported in clinical studies[3,4,27] and in animal models of acute MI.[5,8,28] Recent studies have shown that aldosterone directly induces vascular damage and baroreceptor dysfunction and prevents norepinephrine uptake by the myocardium.[29–31] It is highly plausible that one of the primary targets of aldosterone responsible for post-MI remodeling is the cardiovascular tissue. Our results showed that cardiac aldosterone content was significantly higher in hearts of AT_{1A}-KO mice than in hearts of AT_{1A}-KO sham-operated mice, although concentrations of plasma aldosterone were not significantly different between AT_{1A}-KO sham-operated mice and AT_{1A}-KO MI mice. Similar results were obtained in lisinopril-treated MI and sham-operated mice. Importantly, the severity of LV remodeling seems to be closely associated with cardiac aldosterone levels rather than plasma levels, which did not differ between sham-operated mice and MI mice. Furthermore, our results also show that a relatively low dose (20 mg/kg per day) of spironolactone, which does not affect hemodynamics, can significantly attenuate LV remodeling. Recently, Cohn et al[26] reported sustained reduction of the plasma aldosterone level after renin-angiotensin system blockade using valsartan, but such reduction was independent of the clinical outcome in CHF patients, suggesting the significance of the aldosterone level in the myocardium rather than the level in plasma. Taken together, these previous data and our present results suggest that locally produced aldosterone in post-MI hearts could play a primary role in the pathogenesis of LV remodeling in an autocrine or paracrine manner.

Recent studies have shown that aldosterone has a rapid nongenomic action on many types of cells, including renal epithelial cells and vascular smooth muscle cells.[32] In cardiovascular tissues, it has been suggested that aldosterone may regulate vascular tone via a rapid nongenomic pathway.[33,34] Furthermore, aldosterone has positive inotropic effects on the heart.[35,36] Interestingly, spironolactone itself has similar inotropic effects on isolated working hearts.[36] Although the involvement of these rapid actions in post-MI cardiac function is not clear, their partial involvement in the observed therapeutic effects should be considered because the chronic inotropic effect of spironolactone could facilitate preservation of cardiac function.

Mineralocorticoid receptor antagonist treatment in combination with renin-angiotensin system blockade has been reported to have beneficial effects for patients with severe CHF. Although aldosterone escape could explain the beneficial effect of the combination therapy, the precise molecular mechanism has not been elucidated. Our present findings may help to explain, at least in part, the basis for the beneficial effects of combination therapy. It is highly likely that cardiac aldosterone also plays a critical role in the pathogenesis of heart failure in humans, and clinical use of a mineralocorticoid receptor antagonist, in addition to renin-angiotensin system blockade, could be potentially beneficial as a result of inhibition of the action of cardiac aldosterone produced via an Ang II–independent pathway.

Acknowledgments

This work was supported in part by a grant from Pfizer Inc (to Drs Katada, Saito, and Ohashi). We greatly appreciate Tanabe Seiyaku Co Ltd for kindly providing the experimental animals.

References

1. Garg R, Yusuf S, for the Collaborative Group on ACE Inhibitor Trials. Overview of randomized trials of angiotensin-converting enzyme inhibitors on mortality and morbidity in patients with heart failure. *JAMA*. 1995;273:1450–1456.
2. Pfeffer MA, Swedberg K, Granger CB, Held P, McMurray JJ, Michelson EL, Olofsson B, Ostergren J, Yusuf S, Pocock S. Effects of candesartan on mortality and morbidity in patients with chronic heart failure: the CHARM-Overall programme. *Lancet*. 2003;362:759–766.
3. Pitt B, Zannad F, Remme WJ, Cody R, Castaigne A, Perez A, Palensky J, Wittes J, for the Randomized Aldactone Evaluation Study Investi-

gators. The effect of spironolactone on morbidity and mortality in patients with severe heart failure. *N Engl J Med.* 1999;341:709–717.
4. Pitt B, Remme W, Zannad F, Neaton J, Martinez F, Roniker B, Bittman R, Hurley S, Kleiman J, Gatlin M. Eplerenone, a selective aldosterone blocker, in patients with left ventricular dysfunction after myocardial infarction. *N Engl J Med.* 2003;348:1309–1321.
5. Cittadini A, Casaburi C, Monti MG, Di Gianni A, Serpico R, Scherillo G, Saldamarco L, Vanasia M, Sacca L. Effects of canrenone on myocardial reactive fibrosis in a rat model of postinfarction heart failure. *Cardiovasc Drugs Ther.* 2002;16:195–201.
6. Suzuki G, Morita H, Mishima T, Sharov VG, Todor A, Tanhehco EJ, Rudolph AE, McMahon EG, Goldstein S, Sabbah HN. Effects of long-term monotherapy with eplerenone, a novel aldosterone blocker, on progression of left ventricular dysfunction and remodeling in dogs with heart failure. *Circulation.* 2002;106:2967–2972.
7. Le Menuet D, Isnard R, Bichara M, Viengchareun S, Muffat-Joly M, Walker F, Zennaro MC, Lombes M. Alteration of cardiac and renal functions in transgenic mice overexpressing human mineralocorticoid receptor. *J Biol Chem.* 2001:276:38911–38920.
8. Qin W, Rudolph AE, Bond BR, Rocha R, Blomme EA, Goellner JJ, Funder JW, McMahon EG. Transgenic model of aldosterone-driven cardiac hypertrophy and heart failure. *Circ Res.* 2003:93:69–76.
9. Silvestre JS, Heymes C, Oubenaissa A, Robert V, Aupetit-Faisant B, Carayon A, Swynghedauw B, Delcayre C. Activation of cardiac aldosterone production in rat myocardial infarction: effect of angiotensin II receptor blockade and role in cardiac fibrosis. *Circulation.* 1999;99: 2694–2701.
10. Takeda Y, Yoneda T, Demura M, Furukawa K, Miyamori I, Mabuchi H. Effects of high sodium intake on cardiovascular aldosterone synthesis in stroke-prone spontaneously hypertensive rats. *J Hypertens.* 2001;19: 635–639.
11. Young MJ, Clyne CD, Cole TJ, Funder JW. Cardiac steroidogenesis in the normal and failing heart. *J Clin Endocrinol Metab.* 2001;86: 5121–5126.
12. Xiu JC, Wu P, Xu JP, Guo Z, Lai W, Zhang Y, Li S, Li J, Liu Y. Effects of long-term enalapril and losartan therapy of heart failure on cardiovascular aldosterone. *J Endocrinol Invest.* 2002;25:463–468.
13. Mizuno Y, Yoshimura M, Yasue H, Sakamoto T, Ogawa H, Kugiyama K, Harada E, Nakayama M, Nakamura S, Ito T, Shimasaki Y, Saito Y, Nakao K. Aldosterone production is activated in failing ventricle in humans. *Circulation.* 2001;103:72–77.
14. Yamamoto N, Yasue H, Mizuno Y, Yoshimura M, Fujii H, Nakayama M, Harada E, Nakamura S, Ito T, Ogawa H. Aldosterone is produced from ventricles in patients with essential hypertension. *Hypertension.* 2002;39: 958–962.
15. Silvestre JS, Robert V, Heymes C, Aupetit-Faisant B, Mouas C, Moalic JM, Swynghedauw B, Delcayre C. Myocardial production of aldosterone and corticosterone in the rat: physiological regulation. *J Biol Chem.* 1998;273:4883–4891.
16. Mizuno Y, Yasue H, Yoshimura M, Fujii H, Yamamoto N, Nakayama M, Harada E, Sakamoto T, Nakamura S, Ito T, Shimasaki Y, Ogawa H, Saito Y, Nakao K. Effects of perindopril on aldosterone production in the failing human heart. *Am J Cardiol.* 2002;89:1197–1200.
17. Harada K, Sugaya T, Murakami K, Yazaki Y, Komuro I. Angiotensin II type 1A receptor knockout mice display less left ventricular remodeling and improved survival after myocardial infarction. *Circulation.* 1999;100: 2093–2099.
18. Sugaya T, Nishimatsu S, Tanimoto K, Takimoto E, Yamagishi T, Imamura K, Goto S, Imaizumi K, Hisada Y, Otsuka A, et al. Angiotensin II type 1a receptor-deficient mice with hypotension and hyperreninemia. *J Biol Chem.* 1995;270:18719–18722.
19. Brilla CG, Matsubara L, Weber KT. Advanced hypertensive heart disease in spontaneously hypertensive rats: lisinopril-mediated regression of myocardial fibrosis. *Hypertension.* 1996;28:269–275.
20. Meguro T, Hong C, Asai K, Takagi G, McKinsey TA, Olson EN, Vatner SF. Cyclosporine attenuates pressure-overload hypertrophy in mice while enhancing susceptibility to decompensation and heart failure. *Circ Res.* 1999;84:735–740.
21. Pfeffer JM. Progressive ventricular dilation in experimental myocardial infarction and its attenuation by angiotensin-converting enzyme inhibition. *Am J Cardiol.* 1991;68:17D–25D.
22. Zornoff LA, Matsubara BB, Matsubara LS, Paiva SA, Spadaro J. Early rather than delayed administration of lisinopril protects the heart after myocardial infarction in rats. *Basic Res Cardiol.* 2000;95:208–214.
23. Yoshimura M, Nakamura S, Ito T, Nakayama M, Harada E, Mizuno Y, Sakamoto T, Yamamuro M, Saito Y, Nakao K, Yasue H, Ogawa H. Expression of aldosterone synthase gene in failing human heart: quantitative analysis using modified real-time polymerase chain reaction. *J Clin Endocrinol Metab.* 2002;87:3936–3940.
24. Naruse M, Tanabe A, Sato A, Takagi S, Tsuchiya K, Imaki T, Takano K. Aldosterone breakthrough during angiotensin II receptor antagonist therapy in stroke-prone spontaneously hypertensive rats. *Hypertension.* 2002;40:28–33.
25. Pitt D. ACE inhibitor co-therapy in patients with heart failure: rationale for the Randomized Aldactone Evaluation Study (RALES). *Eur Heart J.* 1995;16(suppl N):107–110.
26. Cohn JN, Anand IS, Latini R, Masson S, Chiang YT, Glazer R. Sustained reduction of aldosterone in response to the angiotensin receptor blocker valsartan in patients with chronic heart failure: results from the Valsartan Heart Failure Trial. *Circulation.* 2003;108:1306–1309.
27. Modena MG, Aveta P, Menozzi A, Rossi R. Aldosterone inhibition limits collagen synthesis and progressive left ventricular enlargement after anterior myocardial infarction. *Am Heart J.* 2001;141:41–46.
28. Cittadini A, Monti MG, Isgaard J, Casaburi C, Stromer H, Di Gianni A, Serpico R, Saldamarco L, Vanasia M, Sacca L. Aldosterone receptor blockade improves left ventricular remodeling and increases ventricular fibrillation threshold in experimental heart failure. *Cardiovasc Res.* 2003; 58:555–564.
29. Wang W. Chronic administration of aldosterone depresses baroreceptor reflex function in the dog. *Hypertension.* 1994;24:571–575.
30. Rocha R, Chander PN, Khanna K, Zuckerman A, Stier CT Jr. Mineralocorticoid blockade reduces vascular injury in stroke-prone hypertensive rats. *Hypertension.* 1998;31:451–458.
31. Barr CS, Lang CC, Hanson J, Arnott M, Kennedy N, Struthers AD. Effects of adding spironolactone to an angiotensin-converting enzyme inhibitor in chronic congestive heart failure secondary to coronary artery disease. *Am J Cardiol.* 1995;76:1259–1265.
32. Boldyreff B, Wehling M. Rapid aldosterone actions: from the membrane to signaling cascades to gene transcription and physiological effects. *J Steroid Biochem Mol Biol.* 2003;85:375–381.
33. Schmidt BM, Oehmer S, Delles C, Bratke R, Schneider MP, Klingbeil A, Fleischmann EH, Schmieder RE. Rapid nongenomic effects of aldosterone on human forearm vasculature. *Hypertension.* 2003;42:156–160.
34. Romagni P, Rossi F, Guerrini L, Quirini C, Santiemma V. Aldosterone induces contraction of the resistance arteries in man. *Atherosclerosis.* 2003;166:345–349.
35. Tanz RD. Studies on the inotropic action of aldosterone on isolated cardiac tissue preparations, including the effects of pH, ouabain and SC-8109. *J Pharmacol Exp Ther.* 1962;135:71–78.
36. Barbato JC, Mulrow PJ, Shapiro JI, Franco-Saenz R. Rapid effects of aldosterone and spironolactone in the isolated working rat heart. *Hypertension.* 2002;40:130–135.

Clinical Course of Arrhythmogenic Right Ventricular Cardiomyopathy in the Era of Implantable Cardioverter-Defibrillators and Radiofrequency Catheter Ablation

Masatoshi KOMURA,[1] MD, Jun-ichi SUZUKI,[1] MD, Susumu ADACHI,[2] MD, Atsushi TAKAHASHI,[3] MD, Kenichiro OTOMO,[4] MD, Junichi NITTA,[5] MD, Mitsuhiro NISHIZAKI,[6] MD, Tohru OBAYASHI,[7] MD, Akihiko NOGAMI,[8] MD, Yasuhiro SATOH,[9] MD, Kaoru OKISHIGE,[10] MD, Hitoshi HACHIYA,[1] MD, Kenzo HIRAO,[1] MD, *and* Mitsuaki ISOBE,[1] MD

SUMMARY

This study investigated the clinical course of arrhythmogenic right ventricular cardiomyopathy (ARVC) patients and in particular evaluated the contribution of radiofrequency catheter ablation (RFCA) and an implantable cardioverter-defibrillator (ICD) to the treatment of ARVC.

ARVC is a myocardial disorder and a cause of sudden cardiac death due to ventricular tachycardia (VT). Little is known about its prognosis in Japanese ARVC patients.

Thirty-five ARVC patients were studied. Mean age of patients whose onset of ARVC was congestive heart failure (CHF) (66.0 ± 4.0 years) was significantly higher than those whose onset was VT (44.5 ± 14.8 years, $P < 0.05$). ARVC patients with CHF onset showed significantly higher death rates compared to those with VT onset. ICD treatment significantly reduced episodes of hospitalization due to VT (0.1 ± 0.4 episodes) in comparison to treatment by RFCA (1.7 ± 2.2 episodes, $P < 0.03$). RFCA treatment did not reduce recurrence of VT in the follow-up period. ICD therapy showed comparable mortality to RFCA treatment.

The prognosis of ARVC with CHF onset is poor. ICD therapy significantly reduced hospitalization due to VT compared with RFCA treatment. ICD implantation in combination with medication may be a better treatment for ARVC. (Int Heart J 2010; 51: 34-40)

Key words: Arrhythmogenic right ventricular cardiomyopathy, Ventricular tachycardia, Implantable cardioverter-defibrillator

Arrhythmogenic right ventricular cardiomyopathy (ARVC) is a rare myocardial disorder characterized by fibro-fatty replacement of the right ventricular myocardium.[1)] It is now well known that ARVC is a cause of sudden cardiac death (SCD) in young people and/or athletes due to ventricular tachycardia (VT).[2)] One of the main goals in the treatment of ARVC is suppression of the VT that results in SCD. Treatment of ARVC is divided into pharmacologic and nonpharmacologic therapies.

The success of drug therapy for control of VT recurrence in ARVC is difficult to evaluate, but the effectiveness of sotalol to suppress the VT has been reported.[3)] Various nonpharmacologic approaches to suppress this VT have been evaluated. Ventriculotomy was performed in the early days, but it resulted in high mortality rates.[4)] Although acute success rates of 60-90% have been reported with radiofrequency catheter ablation (RFCA), VT recurrence is common and may lead to SCD.[5)] Several studies have reported that implantable cardioverter-defibrillator (ICD) therapy prevents SCD by termination of VT.[6-8)] Pharmacologic therapies using sotalol or amiodarone alone or in combination with beta-blockers are considered the first choice of treatment for patients with ARVC.[5)] Thus, implantation of an ICD is recommended in patients with aborted SCD or inducible VT by electrophysiologic study (EPS). RFCA is considered to decrease appropriate intervention of the ICD by partial prevention of VT and to improve quality of life.

The prevalence of ARVC varies widely according to the study population, and the geographic distribution of the disease is controversial.[9)] Hulot, *et al* reported an annual mortality rate of 2.3% and mean age at death of 54 ± 19 years as the natural history of ARVC in France.[10)] Other investigators reported the prognosis of ARVC in Italy, the United States, and Spain. However, little is known about the

From the [1] Department of Cardiovascular Medicine, Tokyo Medical and Dental University Hospital, Tokyo, [2] Department of Cardiology, Shuwa General Hospital, Saitama, [3] Cardiovascular Center, Yokosuka Kyosai General Hospital, Kanagawa, [4] Cardiovascular Department, Ohme Municipal General Hospital, Tokyo, [5] Department of Cardiology, Saitama Red Cross Hospital, Saitama, [6] Department of Cardiology, Yokohama Minami Kyosai Hospital, Kanagawa, [7] Cardiology Division, Musashino Red Cross Hospital, Tokyo, [8] Cardiology Division, Yokohama Rosai Hospital, Kanagawa, [9] Department of Cardiology, National Disaster Medical Center, Tokyo, and [10] Heart Center, Yokohama-City Minato Red Cross Hospital, Kanagawa, Japan.

This study was supported by grants from the Japanese Ministry of Health, Labour and Welfare.

Address for correspondence: Mitsuaki Isobe, MD, Department of Cardiovascular Medicine, Tokyo Medical and Dental University, 1-5-45 Yushima, Bunkyo, Tokyo 113-8519, Japan.

Received for publication March 23, 2009.
Revised and accepted August 21, 2009.

prognosis of Japanese patients with ARVC undergoing ICD implantation or other treatments. It is reasonable to assume that the severity and clinical course of this disease may be different depending on race and geographic region because a variety of genetic factors has been reported. Thus, the aim of this study was to investigate the clinical course of ARVC patients and to evaluate the efficacy of RFCA and ICD in combination with pharmacologic treatment.

Methods

Patients: Patients who were diagnosed as having ARVC at 10 hospitals in the eastern part of the main island of Japan were included in this study. Data were extracted from the medical records of each patient. These included demographic data, clinical data (family history of ARVC or heart disease, initial presentation of the disease, age at onset, physical examination), electrocardiograms (ECG), signal-averaged ECG, holter monitoring, echocardiograms, coronary angiography, left and right ventriculography, endomyocardial biopsy and treatment, and major clinical events.

Thirty-five Japanese patients (26 males and 9 females) were diagnosed as having ARVC on the basis of the standardized criteria for classification of cardiomyopathies recommended by the European Society of Cardiology Working Group on Myocardial and Pericardial Disease and the Scientific Council on Cardiomyopathies of the International Society and Federation of Cardiology (McKenna's criteria).[11] This study protocol was approved by the Ethical Review Board of the Graduate School of Medicine and Dentistry, Tokyo Medical and Dental University.

Group definition: Thirty-five patients were divided into three groups according to the diagnosis at the first hospital visit: CHF group (n = 3), VT group (n = 30), and premature ventricular conductions (PVC) group (n = 2). The VT group was further classified according to the initial treatment for VT: RFCA group (n = 14), ICD group (n = 7), ICD plus RFCA group (n = 5), and medication follow-up group (Med group, n = 4). The RFCA group included 8 patients who underwent RFCA therapy without ICD implantation and 6 patients who underwent RFCA therapy before ICD implantation. All patients in the ICD group underwent ICD therapy and received medication but not RFCA treatment. All patients in the ICD plus RFCA group underwent ICD implantation and RFCA therapy at their initial assessment (Figure 1). Two patients in the PVC group were treated with RFCA therapy, which eliminated their PVCs. They took no antiarrhythmic drugs, and no PVCs or VT have been documented during the follow-up period. Thus, we compared the CHF group and VT group statistically.

Statistical methods: Data are expressed as the mean ± SD for statistical analysis. Student's t-test was used for comparison of age, sex, ECG parameters, duration of follow-up, existence of ventricular wall motion abnormality, and frequency of hospital admission between the VT and CHF groups. Survival rates were estimated by the Kaplan-Meier method and compared by the log-rank test. A P value less than 0.05 was considered statistically significant. All statistical analyses were performed with SPSS statistical software (version 11.0, SPSS Inc., Chicago, Illinois).

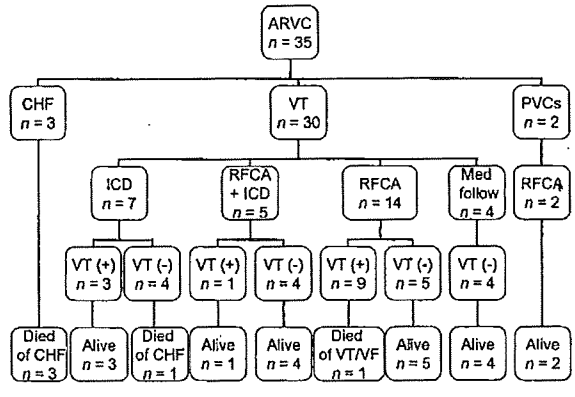

Figure 1. Clinical course of ARVC patients. Patients were divided into the CHF group, VT group, and PVC group. Presence or absence of VT recurrence and current status (dead/alive) are shown.

Results

Patient characteristics: The patient characteristics are described in Tables I and II. The male/female ratio was 2.9 : 1. Mean age at onset was 45.6 ± 15.6 years (range, 15 to 79 years). Average follow-up period from onset was 54.5 ± 48.2 months, and the follow-up period ranged from 1 to 183 months.

Initial symptoms at the onset of ARVC were palpitations (21 patients), syncope (5 patients), dyspnea (3 patients), dizziness (1 patient), shortness of breath (1 patient), and chest pain (1 patient). There were 3 asymptomatic patients at the time of first presentation. Clinical diagnoses at onset were ventricular tachycardia (30 patients, VT group), congestive heart failure (3 patients, CHF group) and PVCs (2 patients) (Table III). One of 35 patients had evidence of a family history of ARVC. Eleven patients had family histories of heart disease: 3 sudden deaths, 3 arrhythmias, 1 congenital heart disease, 1 angina pectoris, and 3 other heart diseases whose details were not described in the medical records. Only 2 patients had a normal 12-lead ECG recording. T-wave inversion in the right precordial leads (V2 and V3) in the absence of right bundle-branch block was recorded in 9 patients, and an Epsilon-wave was recorded in 28 patients. An abnormal signal-averaged ECG was present in 25 of 29 patients. In 22 of the 29 patients, VT was induced by right ventricular myocardial stimulation during EPS. Sixteen patients underwent endomyocardial biopsy, and fibro-fatty replacement was observed in the right ventricular wall in 12 patients.

Twenty-six patients in the VT group were treated with antiarrhythmic drugs including beta-blockers in 16 patients, amiodarone (mean, 164 mg, range, 100 - 200 mg) in 14, sotalol (mean, 120 mg, range, 80 - 160 mg) in 2, procainamide in 2, pirmenol in 2, aprindine in 1, disopyramide in 1, flecainide in 1, cibenzoline in 1, and verapamil in 1, used alone or in combination. The 4 remaining patients did not receive any medication after RFCA because VT could not be induced by EPS performed several months after RFCA

Table I. 35 Patients with ARVC

No.	Age (years)	Sex	Follow up (months)	Symptom	1st diagnosis	ε-wave	LP	ICD and/or RFCA	VT/VF recurrent	VT induction	Medication	Family history	Outcome
1	15	M	19	SOB	VT	(+)	(+)	(-)	(-)	(-)	β-Blocker	Sudden death	
2	16	M	16	Palpitation	VT	(+)	(+)	RFCA	16M	EPS (-)	β-Blocker	Congenital heart disease	Died of VT/VF
3	19	F	146	Cardiomegaly	VT	(+)	(+)	(-)	(-)	EPS (-)	β-Blocker + Aprindine		
4	21	M	10	Abnormal ECG	PVCs	(+)		RFCA	(-)	(-)	(-)		
5	25	M	38	Syncope	VT	(+)	(+)	ICD	3M	RVOT	β-Blocker + Amiodarone	Angina pectoris	
6	27	M	65	Palpitation	VT	(+)	(-)	RFCA + ICD	(-)	RVAP	β-Blocker	Sick sinus symdrome	
7	29	F	36	Syncope	VT	(+)	(+)	RFCA	3M	RVOT	(-)	Sudden death	
8	32	F	183	Chest pain	VT	(+)		RFCA	3M	RVAP & RVOT	Amiodarone + Procainamide		
9	36	M	151	Palpitation	VT	(+)		RFCA → ICD	7M	RVAP	β-Blocker + Procainamide		
10	38	M	97	Palpitation	VT	(+)	(+)	(-)	(-)	EPS (-)	β-Blocker + Disopyramide	Arrhythmia	
11	40	M	12	Abnormal ECG	PVCs	(+)	(+)	RFCA	(-)	(-)	(-)		
12	41	M	14	Dizziness	VT	(-)	(-)	ICD	10M	RVAP	Amiodarone	ARVC	
13	41	M	133	Palpitation	VT	(+)	(-)	RFCA → ICD	66M	RVAP & RVOT	Amiodarone + Flecainide		
14	43	M	48	Palpitation	VT	(+)	(+)	RFCA	23M	RVAP & RVOT	Cibenzoline	Sudden death	
15	45	M	92	Palpitation	VT	(-)	(+)	RFCA	(-)	RV	β-Blocker		
16	45	M	11	Palpitation	VT	(+)	(+)	RFCA	(-)	(-)	(-)		
17	46	M	5	Palpitation	VT	(-)	(+)	RFCA + ICD	(-)	RVAP	(-)		
18	47	M	123	Palpitation	VT	(+)	(+)	RFCA → ICD	4M	RV	Amiodarone + Verapamil		
19	48	F	31	Palpitation	VT	(-)	(-)	RFCA → ICD	3M	RVAP & RVOT	β-Blocker + Amiodarone		
20	49	M	102	Palpitation	VT	(-)	(+)	RFCA → ICD	1M	RVAP & RVOT	β-Blocker		
21	50	M	82	Palpitation	VT	(-)	(+)	RFCA	(-)	(-)	Pirmenol		
22	51	F	29	Palpitation	VT	(+)	(+)	ICD	(-)	RVAP	β-Blocker + Amiodarone	Heart disease	
23	53	M	66	Palpitation	VT	(-)	(+)	RFCA	(-)	RVAP	(-)	Heart disease	
24	55	F	54	Palpitation	VT	(+)	(+)	RFCA + ICD	1M	RVOT	Amiodarone + Pirmenol		
25	56	M	14	Syncope	VF	(+)		ICD	3M	(-)	Sotalol		
26	56	M	17	Syncope	VT	(+)	(+)	ICD	(-)	RVOT	β-Blocker + Amiodarone		
27	57	M	86	Palpitation	VT	(+)	(+)	RFCA	(-)	RVOT	β-Blocker + Amiodarone		
28	58	M	5	Palpitation	VT	(+)	(+)	ICD	(-)	EPS (-)	β-Blocker + Amiodarone		
29	59	F	34	Palpitation	VT	(+)	(+)	ICD	(-)	RVAP	β-Blocker + Sotalol	Heart disease	Died of CHF
30	60	M	59	Syncope	VT	(+)	(+)	RFCA + ICD	(-)	RVOF	β-Blocker + Amiodarone		
31	61	M	52	Palpitation	VT	(+)	(+)	RFCA + ICD	(-)	RVOT	Amiodarone		
32	62	F	1	Dyspnea	CHF	(+)		(-)		EPS (-)	(-)		Died of CHF
33	66	F	49	Dyspnea	CHF	(+)		(-)		EPS (-)	(-)		Died of CHF
34	70	M	5	Dyspnea	CHF	(+)	(+)	(-)		RVOT	(-)		Died of CHF
35	79	M	29	Palpitation	VT	(+)	(+)	(-)	(-)	EPS (-)	Amiodarone		

CHF indicates congestive heart failure; ECG, electrocardiogram; EPS, electrophysiologic study; ε-wave, epsilon wave; ICD, implantable cardioverter-defibrillator; LP, late potential; PVCs, premature ventricular contractions; RFCA, radiofrequncy catheter ablation; RVAP, right ventricular apex; RVOT, right ventricular outflow tract; SOB, shortness of breath; VF, ventricular fibrillation; and VT, ventricular tachycardia.

Table II. Baseline Characteristics

	Overall ($n = 35$)	VT group ($n = 30$)	CHF group ($n = 3$)	P (VT versus CHF)
Age of onset (years)	45.6 ± 15.6	44.5 ± 14.8	66.0 ± 4.0	0.02*
Sex (male : female)	26/9 (2.9 : 1)	23/7 (3.3 : 1)	1/2 (0.5 : 1)	NS
Follow up (month)	54.5 ± 48.2	61.2 ± 48.5	18.3 ± 26.6	NS
(i or c) RBBB	17/35	14/30	2/3	NS
ε-Wave	28/35	23/30	3/3	NS
Negative-T	9/35	8/30	1/3	NS
RV dilatation	23/29	22/27	1/2	NS
LV dysfunction	3/32	1/27	2/3	NS
CVD	5/35	2/30	3/3	< 0.001*

CVD indicates cardiovascular death; ε-wave, epsilon-wave; (i or c) RBBB, incomplete or complete right bundle-branch block; negative-T, negative-T wave in V_2 or V_3; RV, right ventricle; and LV, left ventricle.

Table III. Initial Symptoms and Diagnosis

Initial symptoms		Clinical diagnosis	
•Palpitations	21	•VT	30
•Syncope	5	•CHF	3
•Dizziness	1	•PVCs	2
•SOB	1		
•Chest pain	1		
•Dyspnea	3		
•Abnormal ECG	2		
•Cardiomegaly	1		
	Total 35 pts		Total 35 pts

CHF indicates congestive heart failure; ECG, electrocardiogram; pts, patients; PVCs, premature ventricular contractions; SOB, shortness of breath; VT, ventricular tachycardia.

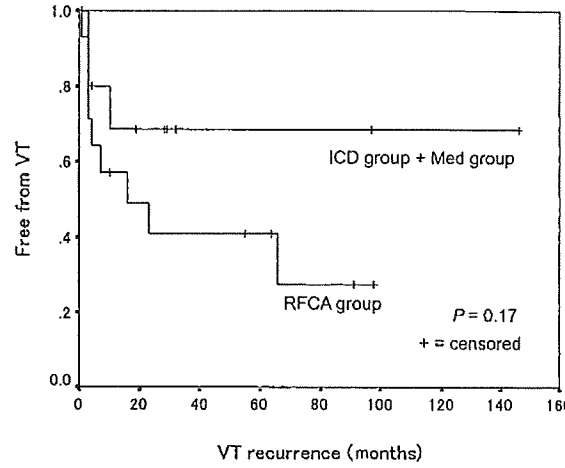

Figure 2. Kaplan-Meier curve of duration of freedom from VT recurrence post RFCA. Duration without VT recurrence after RFCA therapy was not significantly different from that in patients not undergoing RFCA therapy.

in 3 of the patients and because the other patient wanted to get pregnant. Four patients out of 35 died of progressive heart failure, and one patient died of VT/VF recurrence (Figure 1).

VT group: Palpitations and syncope were the most common presenting symptoms in the VT/VF group. Fifteen of the 30 patients were transferred to the emergency room with VT as the manifestation of the disease and received treatment to terminate the VT by direct current cardioversion, automated external defibrillator, or antiarrhythmic drug infusion. Mean age at onset in this group was 44.5 ± 14.8 years. Twenty-three of 30 patients were male.

The clinical course of patients included in the VT group is described in Figure 1. Five patients underwent RFCA plus ICD therapy at the first assessment. One of these 5 patients had at least one episode of VT recurrence after the RFCA and ICD therapy. Fourteen patients received RFCA therapy without ICD therapy for VT at first assessment (RFCA group). Mean duration from first visiting our hospitals to RFCA was 15.2 ± 44.4 months (range, 1 to 168 months) and the median was 2.0 months. One patient visited a hospital in August 1991 and received RFCA therapy in August 2005. During the follow-up period VTs recurred in 9 of these patients. One patient died at 18 years of age from VT/VF that occurred during exercise 16 months after RFCA therapy. An ICD was implanted in 6 patients in the RFCA group after recurrence of VT or a second or third session of RFCA therapy. The average period from first RFCA therapy to ICD implantation was 43.0 ± 25.5 months. Second RFCA therapy was performed in 6 patients, and third RFCA therapy was performed in 2 patients. Five of the 6 patients who underwent a second or third session of RFCA therapy also underwent ICD implantation.

All 19 patients in the VT group underwent RFCA therapy for VT, and VT recurred in 10 (52.6%) of these 19 patients. The mean period from RFCA therapy to VT recurrence was 14.0 ± 20.1 months (range, 1 to 66 months). Average duration of follow-up in the 9 patients free from VT recurrence was 57.6 ± 31.0 months (range, 5 to 92 months). Among the 10 patients with VT recurrence, 1 received a beta-blocker only, 2 received a beta-blocker with another antiarrhythmic drug, 1 received a beta-blocker with amiodarone, and 3 received amiodarone with another antiarrhythmic drug. In the 9 patients without recurrence of VT, 2 received a beta-blocker only, 2 received a beta-blocker with amiodarone, and 1 received amiodarone alone. There was no significant difference in medications between

the two groups.

Seven patients who did not undergo RFCA therapy were implanted with ICD (ICD group), and one died of progressive heart failure without VT recurrence 32 months after implantation. In total, 18 of the 30 VT group patients underwent ICD implantation. At least one episode of VT recurred in 6 of these 18 patients (33.3%), and they received appropriate ICD intervention.

The 4 patients not undergoing RFCA nor ICD therapy for VT were categorized into the Med group. These patients received beta-blocker alone, beta-blocker with aprindine, beta-blocker with disopyramide, or amiodarone alone.

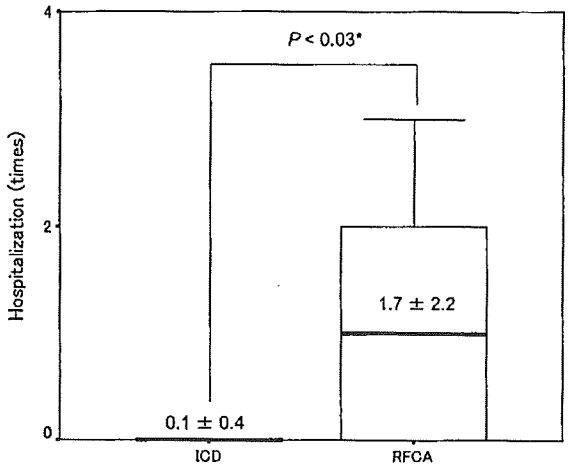

Figure 3. Number of episodes of hospital admission due to VT recurrence. The average number of episodes of hospital admission for treatment of VT was significantly lower in the ICD group (mean, 0.1 ± 0.4; range, 0 to 1 episodes) than in the RFCA group (mean, 1.7 ± 2.2,; range, 0 to 7 episodes).

Mean follow-up duration in this group was 72.6 ± 59.9 months. Cardiac events including SCD, hospitalization, or visiting an emergency room due to VT or CHF did not occur in the follow-up period.

Comparison of duration from the initial therapy to recurrence of VT between the RFCA group and the ICD group plus the Med group is shown in Figure 2. Duration without VT recurrence and rate of VT recurrence after ICD or RFCA therapy were not significantly different. Mean duration from RFCA/ICD to VT recurrence was 12.7 ± 20.1 months in the RFCA group and 5.3 ± 4.0 months in the ICD group ($P = 0.45$). In this study, one patient died of VT/VF in the RFCA group, and one patient died of CHF in the ICD group. ICD therapy showed no improvement in mortality over that of RFCA in this study. However, ICD therapy did reduce the episodes of hospitalization compared with RFCA therapy. The average number of episodes of hospitalization was 0.1 ± 0.4 (range, 0 to 1 episodes) in the ICD group and 1.7 ± 2.2 (range, 0 to 7 episodes) in the RFCA group (Figure 3).

CHF group: The symptom at the onset of ARVC in the 3 patients comprising the CHF group was dyspnea with increasing cardiothoracic ratio on chest X-ray film. RV dilatation with hypokinesis was observed in all patients by echocardiography. Two patients had diffuse severe hypokinesis of the left ventricular wall and died of progressive heart failure. One patient recovered from CHF with conservative therapy and showed good LV function by left ventricular angiography (left ventricular ejection fraction (LVEF) = 72%), but 5 months later, he was rehospitalized and died of CHF. All patients in this group had at least one episode of nonsustained VT without hemodynamic collapse. None were treated with antiarrhythmic drugs. Mean age at onset in the CHF group was 66.0 ± 4.0 years. Duration of follow-up was 18.3 ± 26.6 months. Autopsy diagnosis was established in all CHF group patients. Fibro-fatty replacement was observed in both the right ventricular and left ventricular walls in all patients. Pathologic diagnosis

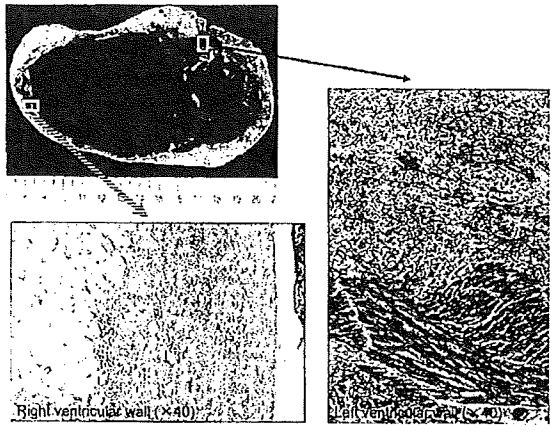

Figure 4. Representative histologic sections at autopsy from a patient with ARVC who died of progressive heart failure. Fibro-fatty replacement and inflammatory cell infiltration were observed in both ventricular walls. Fibro-fatty replacement was more dominant in the right ventricular than the left ventricular wall.

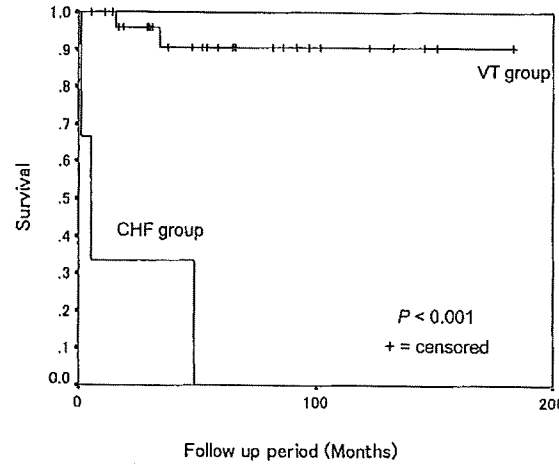

Figure 5. Kaplan-Meier survival curves. The CHF group showed a significantly higher mortality rate in comparison to the VT group ($P < 0.001$).